



universität
wien

MASTERARBEIT / MASTER'S THESIS

Titel der Masterarbeit / Title of the Master's Thesis

„Sphingosine Kinase I is a novel target in lung adenocarcinoma“

verfasst von / submitted by

Margarita Kurnaeva

angestrebter akademischer Grad / in partial fulfilment of the requirements for the degree of
Master of Science (MSc)

Wien, 2022 / Vienna, 2022

Studienkennzahl lt. Studienblatt /
degree programme code as it
appears on
the student record sheet:

UA 066830

Studienrichtung lt. Studienblatt /
degree programme as it appears
on
the student record sheet:

Masterstudium Molekulare Mikrobiologie,
Mikrobielle Ökologie und Immunbiologie

Betreut von / Supervisor:

Univ.Prof. Dr. Emilio Casanova

Table of contents

Table of contents	3
Acknowledgements	6
Abstract	7
Zusammenfassung	8
List of abbreviation	9
Introduction	10
Lung cancer	10
Diagnostic	11
Risk factors and molecular biology of lung cancer	11
KRAS-associated tumor biology	12
EGFR-associated adenocarcinomas	14
Tumor microenvironment	16
Current treatment of lung cancer	17
Surgery	17
Chemotherapy	17
Radiotherapy	17
Targeted drug therapy	18
Immune checkpoint inhibitors (ICIs)	18
Combined therapies	19
Sphingosine kinase I and cancer	20
Multifactorial role of sphingosine-1-phosphate	20
Sphingosine kinases and S1P	21
Sphingosine kinases 1 and cancer	22
Aims of this study	24
Materials and Methods	25
Mammalian cell lines	25
Cell culturing medium	25
Freezing cells	25
Thawing cells from liquid nitrogen stock	26
Counting cells	26
Transfection	26
Lentivirus generation	26
Bacterial cell lines	27
Competent cells preparation	27

Transformation and plasmid isolation	27
CRISPR-Cas9 knock-out of Sphingosine kinase 1 gene	28
Preparation of guide RNA	28
Generation of pools	30
DNA isolation	30
PCR amplification	31
Agarose gel electrophoresis	31
Purification of PCR fragments	31
Sequencing of PCR product	32
Generation of single clones	32
Real-time PCR	32
RNA extraction	32
Reverse transcriptase-PCR (RT-PCR)	33
Quantitative real-time PCR (qPCR)	33
Western blotting	36
Cells preparation for protein isolation	36
BCA assay	36
Samples preparations and SDS-PAGE	37
Semi-dry transfer	38
Antibody detection	39
Cell-based assays	39
Cell proliferation assay	39
Wound-healing assay	39
Lentiviral transduction of KP and KP Δ SK1 cell line	40
Scratch assay with fluorescently labeled cells	40
Proliferation assay	40
Rescue experiment	41
Transwell and invasion assays	42
Results	43
Generation of KP cells deficient in SK1 expression	43
Cells lacking SK1 exhibited changed morphology with profound movement and filopodia formation	44
Cells deficient in SK1 demonstrated reduced proliferation efficiency	45
KP Δ SK1 cells showed random cell motility and lack of monolayer formation	47
Sphingosine-1-phosphate is not able to rescue the proliferation capacity of KP Δ SK1 cells	49

KP Δ SK1 cells exhibited increased movement but reduced invasiveness compared to KP cells	50
KP Δ SK1 cells revealed specific expression profile	52
Discussion	53
Morphologic description of KP cancer cells lacking SK1	54
SK1 ablation leads to reduced proliferation, invasiveness and increased motility	55
S1P is not able to rescue KP Δ SK1 cellular phenotype	57
Conclusion and outlook of this study	57
References	59
Supplementary figures	66

Acknowledgments

This work is foremost dedicated to my husband, who never stops reminding me to smile and keep going despite difficulties during my Master's thesis time. Secondly, I am deeply thankful to our head of laboratory Dr. Emilio Casanova with his constant scientific and organisational support and frequent exclamation: "Any breakthrough?" and to Dr. Herwig Moll for his ideas and brainstorming in this research. Thirdly, I am filled with gratitude to my peers Monica and Corina for the help I have received regardless of whether they were scientific or personal. Lastly, I thank all other lab members for the assistance they provided.

Abstract

In spite of the advances in cancer treatment, lung cancer remains one of the leading death drivers among cancer patients, with lung adenocarcinoma (LUAD) accounting for ~40% of diagnoses. Data from cancer patients showed the overexpression of sphingosine kinase 1 (SK1) in lung cancer along with other cancer types. Particularly in LUAD lung cancer patients, SK1 overexpression promotes significant resistance to doxorubicin chemotherapy leading to a poor prognosis. Moreover, increased SK1 levels led to cancer relapse in LUAD patients treated with adjuvant chemotherapy. This is generally associated with the advanced clinical stage of the disease and as a consequence with a shorter survival rate. Hence, additional approaches are needed to improve the outcome and prognosis of LUAD patients with particularly KRAS-mutated cancers, which accounts to almost 30% of all lung adenocarcinomas and are notoriously difficult to treat.

To dissect the biological role of SK1, we generated knock-out cell line lacking SK1 expression in KRAS-mutated adenocarcinoma cells. These cells were characterised using various functional assays, including wound-healing, proliferation and transwell assays. We found that deletion of SK1 led to increased cellular motility, filopodia/lamellipodia-like formation and reduced proliferation capacity. Moreover, we demonstrated that biological mechanism of SK1 was cell intrinsic. In addition, we observed reduced invasiveness of these cells potentially due to downregulation of *Fascin 1* expression and vital cell-cell adhesion genes, *Cdh1* and *Cdh2*. Although the mechanism of increased cell motility is yet to be studied, our data suggests that SK1 can indeed be a promising target in lung cancer treatment.

Zusammenfassung

Trotz der Fortschritte in der Krebsbehandlung ist Lungenkrebs nach wie vor eine der häufigsten Todesursachen bei Krebspatienten, wobei das Lungenadenokarzinom (LUAD) etwa 40 % der Diagnosen ausmacht. Daten von Krebspatienten haben gezeigt, dass die Sphingosinkinase 1 (SK1) bei Lungenkrebs und anderen Krebsarten überexprimiert ist. Insbesondere bei LUAD-Lungenkrebspatienten fördert die Überexpression von SK1 eine signifikante Resistenz gegen die Doxorubicin-Chemotherapie, was zu einer schlechten Prognose führt. Außerdem führen erhöhte SK1-Werte bei LUAD-Patienten, die mit einer adjuvanten Chemotherapie behandelt werden, zu einem Rückfall des Krebses. Dies ist in der Regel mit einem fortgeschrittenen klinischen Stadium der Krankheit und folglich mit einer kürzeren Überlebensrate verbunden. Daher sind zusätzliche Ansätze erforderlich, um das Ergebnis und die Prognose von LUAD-Patienten mit besonders KRAS-mutierten Krebsarten zu verbessern, die fast 30 % aller Lungenadenokarzinome ausmachen und bekanntermaßen schwer zu behandeln sind.

Um die biologische Rolle von SK1 zu entschlüsseln, haben wir Knock-out-Zelllinien erzeugt, denen die SK1-Expression in KRAS-mutierten Adenokarzinomzellen fehlt. Diese Zellen wurden mit verschiedenen Funktionstests charakterisiert, darunter Wundheilungs-, Proliferations- und Transwell-Tests. Wir stellten fest, dass die Deletion von SK1 zu einer erhöhten Zellmotilität, zur Bildung von Filopodien/Lamellipodien und zu einer verminderten Proliferationsfähigkeit führte. Darüber hinaus konnten wir nachweisen, dass der biologische Mechanismus von SK1 zellinterner Natur ist. Darüber hinaus beobachteten wir eine verringerte Invasivität dieser Zellen, die möglicherweise auf eine Herunterregulierung der Expression von Fascin 1 und der wichtigen Zell-Zell-Adhäsionsgene *Cdh1* und *Cdh2* zurückzuführen ist. Obwohl der Mechanismus der erhöhten Zellmotilität noch untersucht werden muss, deuten unsere Daten darauf hin, dass SK1 tatsächlich ein vielversprechendes Ziel für die Behandlung von Lungenkrebs sein kann.

List of abbreviations

LUAD - lung adenocarcinoma

NSCLG - non-small cell lung cancer

SK1 - sphingosine kinase 1

S1P - sphingosine 1 phosphate

ICI - immune checkpoint inhibitors

EGFR - epidermal growth factor receptor

KRAS - v-Ki-ras2 Kirsten rat sarcoma

CTLA-4 - cytotoxic T lymphocyte associated protein 4

PD-1 - programmed cell death 1

PD-L1 - programmed cell death ligand 1

Introduction

Our body consists of trillions of cells which in a well-organized fashion undergo growth, division, and eventually programmed death. Sometimes, this cycle is disrupted by changes in growth patterns leading to extensive proliferation and occasionally to cancer. Although many different types of cancer have been described and scientific advances have increased the life expectancy of cancer patients, hardly any cancer types can be completely cured. This is the case of lung cancer which according to the American Lung Association is not only the most common incident cancer type but also the leading cause of death among both men and women in the US (www.lung.org). In Europe, the lung cancer incidence varies with a country with the highest prevalence in Hungary accounting for 56.7 cases per 100000 people of both genders (www.wcrf.org). In Austria, lung cancer was the most common cancer-related mortality among men and the second among women in 2017 and continues to be a major health problem nowadays [1].

Lung cancer

Lung cancer is broadly divided into two groups: small cell lung cancer (SCLC) and non-small cell lung cancer (NSCLC). This division is based upon the microscopic appearance of cancer cells, their growth pattern, and spread. Around 10-15 % of all lung cancer incidences contribute to SCLC and 80-85 % are NSCLC [2,3]. Based on the cell origin, NSCLC is further subdivided into adenocarcinoma (ADC), squamous cell carcinoma, large cell carcinoma, and less common adenosquamous carcinoma and sarcomatoid carcinoma (Fig. 1). Adenocarcinomas are the most prevalent type of cancer contributing to >30 % of all lung cancer types and almost half of all NSCLC. SCLCs subdivided into small cell carcinoma and combined small cell carcinoma. SCLC is considered the most aggressive type due to quick growth and spread compared to NSCLC. Nevertheless, SCLC responds well to both chemotherapy and radiotherapy (<https://www.cancercenter.com/>).

Lung epithelium contains stem cells and diverse progenitor cells which give rise to different cell populations. Ciliated, non-ciliated, basal, and mucosal cells cover the major airways and produce mucus to lubricate and protect the lungs. The actual gas exchange occurs in alveoli which are lined with alveolar type I and type II cells. The SCLC and NSCLC have been shown to have different progenitors [4]. Since lung cancer

is a heterogeneous disease with abundant mutations exceeding any other cancer types [5], the exact origin of these types of lung cancer largely remains unknown.

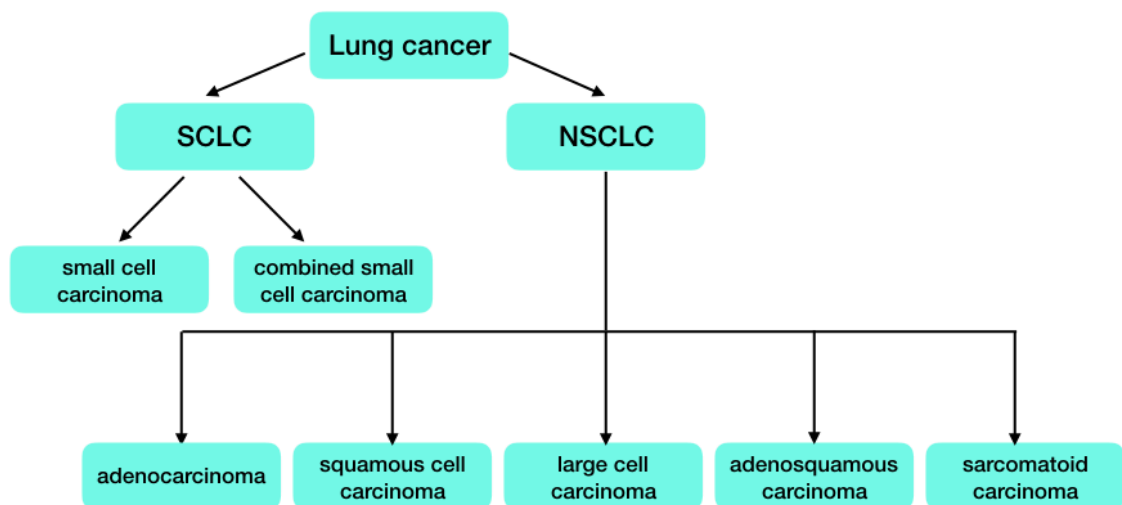


Figure 1. Subdivision of lung cancer types.

Diagnostic

X-Ray or computed tomography are initial imaging modalities in patients suspected of lung cancer. Positron emission tomography and magnetic resonance imaging are usually used to confirm the previous analysis [1]. In the case of observed nodule growth, the tissue sample might be collected by a bronchoscope for histological analysis. In Austria, the primary method for lung cancer diagnoses is bronchoscopy (87.9%) [6]. In the advent of molecular diagnostics, the histological samples can be further used for specific marker determination to distinguish a particular type of lung cancer. Sputum cytology is also used but is most helpful if cancer affects major airways of the lungs, otherwise, other methods are used (www.cancer.org).

Risk factors and molecular biology of lung cancer

The most common and predominant cause of lung cancer is smoking (including passive), followed by radon exposure, pollution, hazardous chemical substances such as asbestos, and genetic predisposition [7,8]. Exposure to these factors can lead to genetic alterations in epithelial lung cells. Such alterations can usually occur in oncogenes or tumor suppressors affecting their signaling pathways. The mutations have been found in epidermal growth factor receptor (*EGFR*), v-Ki-ras2 Kirsten rat sarcoma (*KRAS*), v-Raf murine sarcoma viral oncogene homolog B (*BRAF*), receptor tyrosine-protein kinase erbB-2 (*HER2*), cellular tumor antigen p53 (*p53*), and many other oncogenes and tumor suppressors [9]. It should be noted that the development of lung

cancer is a multi-step process acquiring genetic aberrations over time, thus giving survival and growth advantage over non-mutated cells [10].

The genetic alterations driving tumor growth are best studied in lung adenocarcinomas (LUAD) since this is the most common type of lung cancer. The EGFR-associated adenocarcinomas are more prevalent among the East-Asian population accounting for almost 55%, while in Europe and the US this figure stands around 15% (Fig. 2). In contrast, KRAS-associated LUADs contribute to 20-30% in Europe/US and 8-10% in East Asia [11].

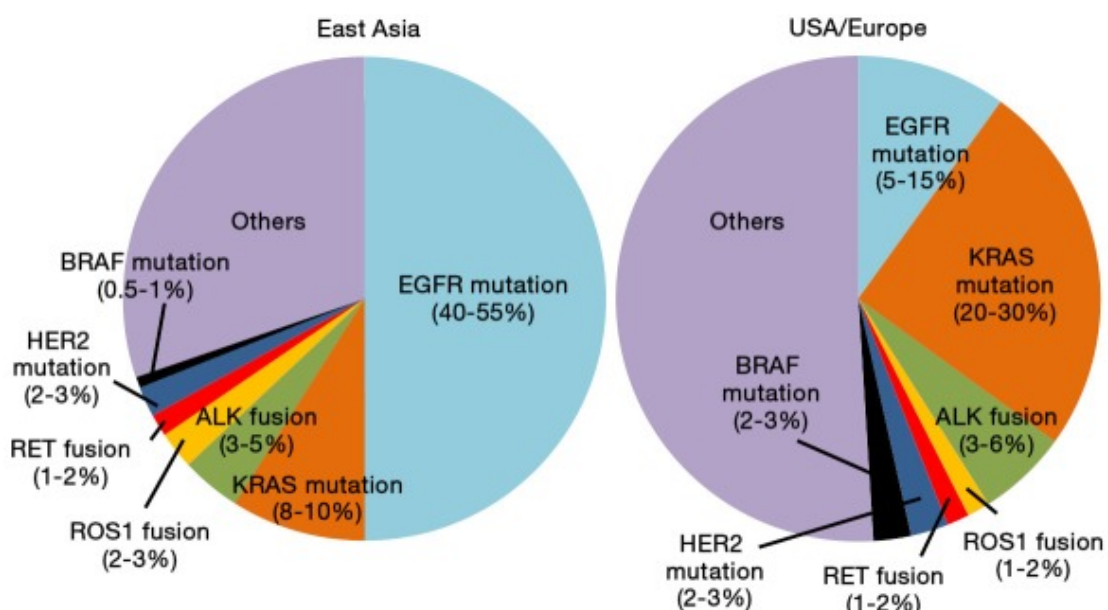


Figure 2. Lung cancer worldwide incidence. Adenocarcinomas are the most prevalent lung cancers with 40-55% of EGFR-associated LUAD detected in East Asian population and 5-15% among European/ North American populations. KRAS-associated LUACs are more prevalent in USA and Europe (20-30%) while in East Asia these figure is almost three times less [11].

KRAS-associated tumor biology

KRAS is the most frequently mutated protein in lung cancer accounting for ~30% in LUAD and ~15% in all lung cancer types (Fig. 2). It is a member of the RAS family which belongs to the large superfamily of GTPases. The RAS family controls cell growth, proliferation and includes also HRAS and NRAS proteins. The knock-out experiments in mice showed that KRAS is the most vital member of the RAS family and its presence is critical for proper mouse development [12].

The activation of KRAS depends on its bound state to either GTP, thus participating in downstream signalling, or to GDP, causing its inactive form [13]. This

ratio is tightly controlled in healthy cells [14]. However, in cancer cells, mutated KRAS is locked in a constitutively GTP-bound active state [15]. The mutations supporting active KRAS-GTP state are the most common aberrations in LUAD constituting 20-40% of all cases [16].

The three amino acid positions G12, G13, and Q61 were shown to be a hotspot for KRAS mutation. The G12 mutation makes up to ~ 83% of all cases, while G13 and Q61 comprise 14% and 2%, respectively [17]. In LUAD, only G12 mutations are known with the most prevailing (~46%) being G12C (Fig.3) [18].

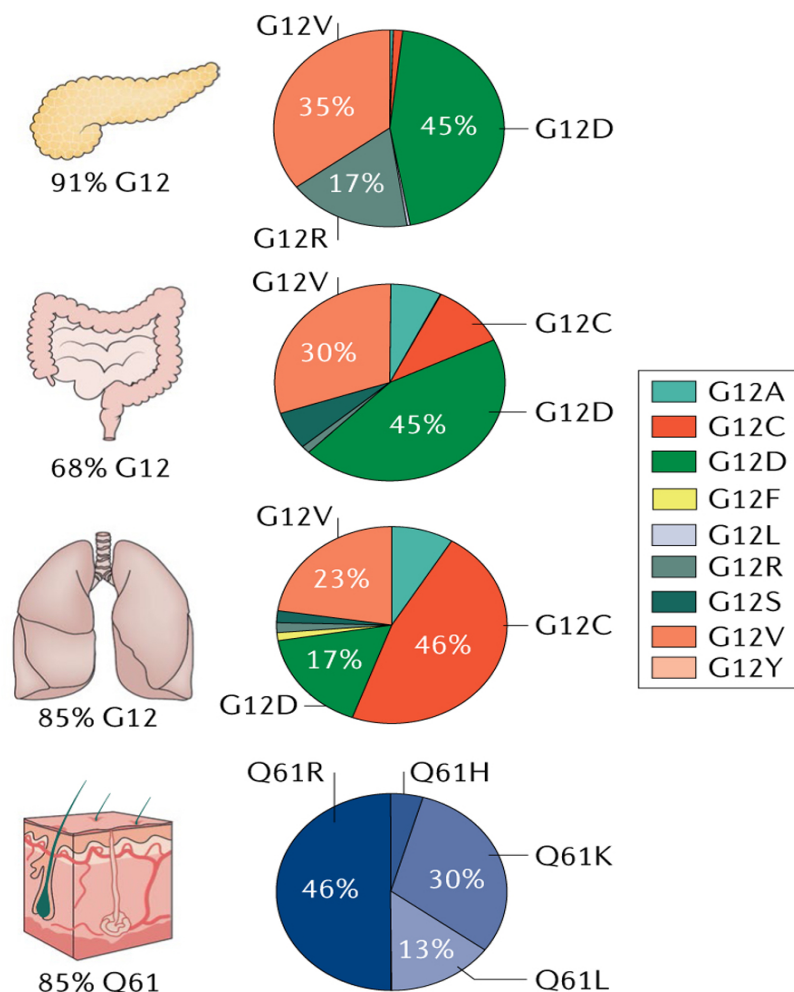


Figure 3. Percentage of C12 mutations in KRAS. In KRAS, three amino acid positions G12, G13 and Q61 are frequently mutated leading to formation of adenocarcinomas. The most prevalent however are G12 in pancreatic ductal, colorectal and lung adenocarcinomas and Q61 in melanoma. In lung adenocarcinoma G12 mutation with its substitution to C (KRAS^{G12C}) constitutes to almost 85% in ~ 46% cases. Adapted from [18].

Despite its common frequency and extensive research, KRAS-driven tumors remain notoriously difficult to treat. This is due to the high affinity of KRAS to GTP while its inhibition can affect many other vital protein families which rely on GTP energy for proper functioning [15,19]. Additionally, KRAS-driven tumors are linked to tumor-

associated inflammation due to insulting epithelial cells with inflammatory cytokines over the course of time [20]. Rather than directly targeting only KRAS, researchers have been paying more attention to downstream effector pathways activated by KRAS. This led to generation of a plethora of selective inhibitors against KRAS downstream effectors like RAF/MEK/ERK and PI3K/AKT/mTOR. A handful of MEK inhibitors are approved for BRAF-mutant melanoma treatment [21]. However, in clinical studies, the usage of single RAF, MEK, and ERK inhibitors failed to affect KRAS-associated LUAC. This is not a surprise since RAS influences multiple downstream signalling pathways and inhibition of just one member will lead to activation of another downstream molecule if not several. Thus, the combination of inhibitors against both downstream and upstream members may play an outcome [19].

The relatively preserved intrinsic GTP-hydrolysis rate of the KRAS^{G12C} mutant allowed a generation of direct inhibitors against KRAS^{G12C} [19]. Two drugs AMG 510 (sotorasib) and MRTX849 (adagrasib) showed vigorous pre-clinical efficacy. In May 2021, sotorasib was approved by FDA in the US as the first drug against NSCLC KRAS^{G12C} [19,22–24]. However, due to the intrinsic nature of cancer cells towards the rapid mutation, the monotherapy eventually will lead to the tumor escape. In addition, the NSCLC KRAS-associated tumors are usually accompanied by mutations in tumor-suppressor genes like p53 [25] challenging modern therapies. Thus, a combination of drugs targeting different KRAS effectors and direct inhibitors of mutated KRAS are needed.

EGFR-associated adenocarcinomas

EGFR is a member of the epidermal growth factor receptors family, ErbB, which also includes HER2/neu, Her 3, and Her 4. EGFR is a transmembrane tyrosine kinase protein positioned upstream of RAS. Upon stimulation, EGFR is activated and the signal is transduced through RAF/MEK/ERK, PI3K/AKT/mTOR, and JAK/STAT pathways [16,26]. These downstream signalling pathways lead to cell survival and proliferation (Fig. 4). Activating mutations in EGFR gene are involved in many pathologies and particularly in NSCLC [27,28]. There are three classes of EGFR mutations: short in-frame deletion in exon 19, single nucleotide substitution from exon 18 to 21, and in-frame duplications or insertions in exon 20 [29]. Around 80% of all mutations occur in exon 19 and single L858R substitution in 21 exon [30]. Most of these mutations are commonly found in younger female patients with no smoking history [16].

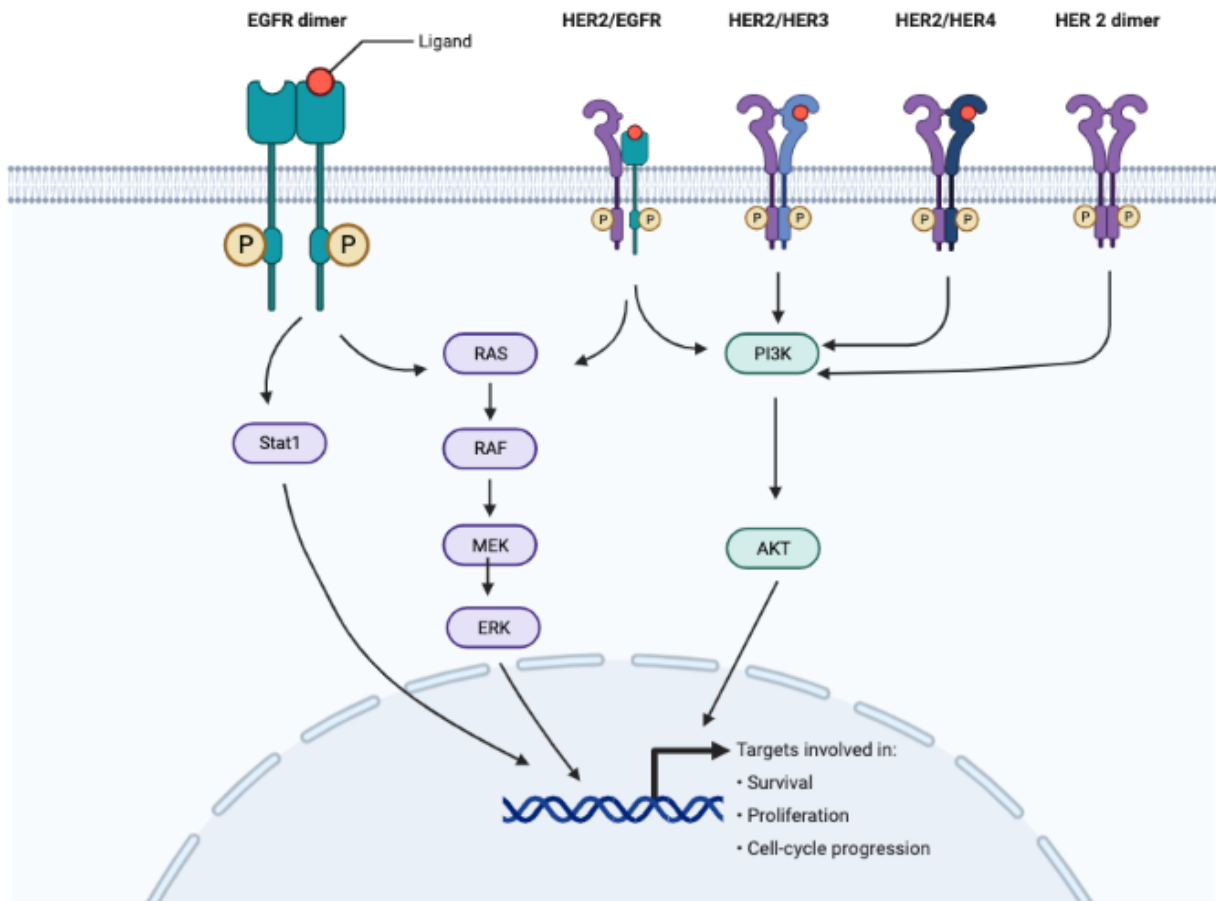


Figure 4. EGFR signalling cascade. Epidermal Growth Factor receptor (EGFR) is responsible for activation of vital processes linked largely to the cellular proliferation and inhibition of apoptosis. The EGFR family includes ErbB2/HER2/Neu, ErbB3/HER3, and ErbB4/HER4 members. Upon binding of its ligand, homo- or heterodimerization occurs causing activation of one or more downstream signalling pathways such as PI3K/AKT, MAPK, and STAT. Created with BioRender.com [www.biorender.com].

Two tyrosine kinase inhibitors (TKIs), erlotinib and gefitinib, were discovered before somatic mutations in the EGFR gene were known. Scientists noted that younger female cancer patients without or with modest smoking history responded to TKIs. The follow-up studies confirmed that somatic EGFR mutations are strongly associated with the positive response to TKIs therapy among cancer patients (reviewed in [31]). These first TKIs reversely bind the ATP-binding site of the EGFR kinase domain with high specificity towards activating mutations, thus inhibiting EGFR's activity. Currently, erlotinib and gefitinib are approved for the treatment of NSCLC [32].

The second-generation TKIs, afatinib and dacomitinib, are irreversible pan-ErbB inhibitors. Application of first- and second-generation TKIs eventually lead to tumor resistance via secondary mutation T790M in the tyrosine kinase domain. T790M was found in ~40% of patients treated with these TKIs [16]. Osimertinib is the third-generation TKI which selectively binds active L858R and T790M EGFR and is

approved for the treatment of patients who develop acquired TKI resistance from erlotinib, gefitinib, afatinib, and dacomitinib treatment [33]. Despite the clinical significance, there are patients who developed resistance towards osimertinib, hence new approaches to treat these cancer patients are of utmost importance [34].

Tumor microenvironment

Inflammation is considered a major co-factor in cancer biology. The tumor cells can promote local inflammation and concurrently elude the host's immunological response. Paradoxically, the immune system can play the so-called "yin/yang" both antagonizing and amplifying tumor development and progression [35]. By doing so, it can provide tumors with vital signalling molecules, growth, survival, and angiogenesis factors. Simultaneously, cancer cells communicate with each other by direct cell-to-cell interactions or via cytokines release, thus shaping their microenvironment [36]. This paradox has been explained by the concept of "3Es immunoediting" (Fig.5) [37].

At the first elimination stage, the immune system eliminates cancer cells. The second stage is a phase of equilibrium when the immune system is unable to fully clear cancer clones, thus putting selective pressure on cancer clones. In the last escape stage, the cancer cells adapt to the immune pressure and develop the ability to evade it and uncontrollably divide. This concept explains the importance of the tumor microenvironment in cancer development and progression [38].

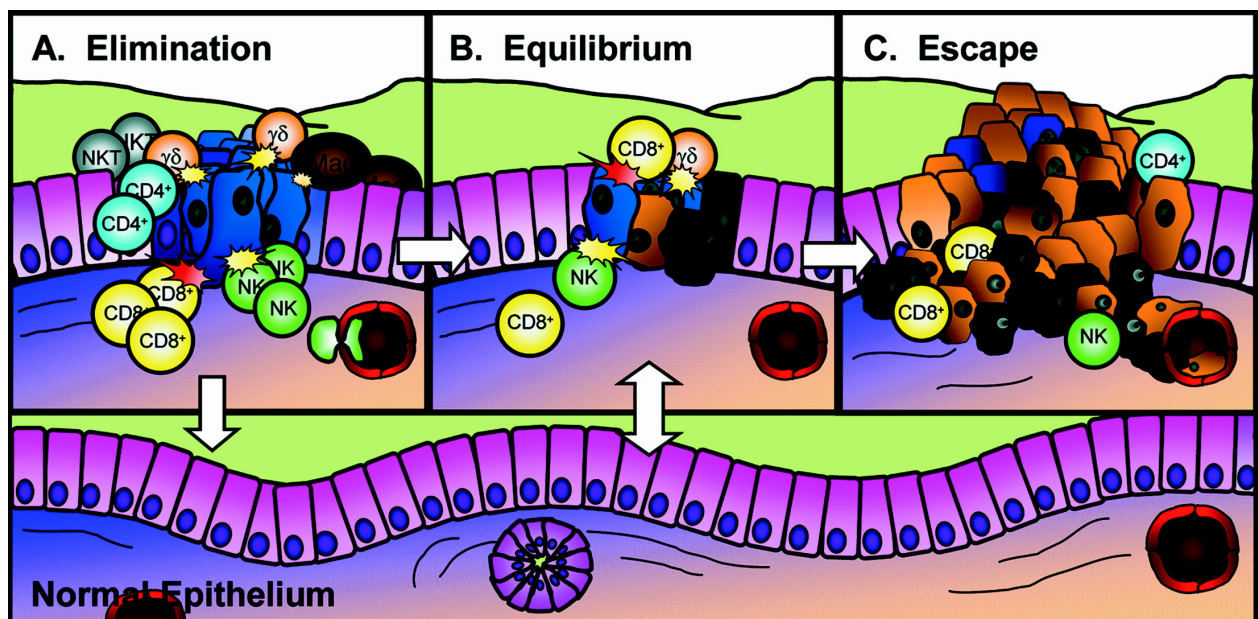


Figure 5. The concept of three ES immunoediting in cancer. It involves dynamic process of immunological surveillance and tumor progression comprised of three phases: elimination, equilibrium

and escape. During elimination stage, cancer cells are cleared by immune cells. In the equilibrium phase, the immune system releases potent selective molecule to target any survived cancer cells, thus keeping the proliferation of cancer cells, however not completely eliminating them. In the escape phase, tumor clones which survived equilibrium phase can grow leading to tumor progression [37].

Current treatment of lung cancer

Surgery

Thoracic surgery plays a vital role in lung cancer treatment and is usually the best option if the tumor is small and has not metastasised yet. This may follow radio and chemotherapy to keep the tumor cells at bay. Still, due to the late diagnostics, the thoracic surgery application may not be an optional treatment rather the best diagnostic tool for molecular determination of tumor subtypes. In the era of personalised medicine, thoracic surgery can help to assess acquired resistance to targeted therapy [39].

Chemotherapy

Chemotherapy remains an essential component of lung cancer treatment [40]. These are toxic compounds designed to kill dividing cells, however, these compounds lack cancer cell specificity and thus affect normal cells too. Nevertheless, this toxicity is overcome by tumor reduction and prolonged life span. Although chemotherapy alone eventually plateaued its benefit, it is the only systemic therapy with confirmed enhanced outcomes, particularly in patients with metastatic diseases and when administered along with immunotherapies [40].

Radiotherapy

Radiotherapy is a non-surgical option for lung cancer treatment. It involves the use of high-energy beams to directly kill cancer cells via either external or internal radiation. The external radiation treatment is performed outside the body directing the beam to the area affected by cancer. Internal radiation is also called endobronchial radiotherapy when a radioactive implant is placed directly into the tumor or near the tumor via bronchoscope and radiation is emitted into the affected area. However, after initial advances in tumor suppression following radiotherapy, the majority of patients suffer from cancer relapses and metastasis [41]. Thus, radiotherapy is nowadays used in conjunction with other methods, like thoracic surgery, chemotherapy, and immunotherapy.

Targeted drug therapy

The advent of mutated cancer driver genes discovery has revolutionised our vision of lung cancer heterogeneity. Based on specific oncogene mutation(s), researchers were able to specify signalling pathways affected by this mutation(s). This made it possible to determine key players which can be targeted to inhibit the growth, progression, and metastasis of cancer cells, like RAF and MEK kinases in the MAPK pathway. Although initial success in NSCLC patients was promising [42], the application of targeting therapy alone eventually led to secondary mutations or activation of compensatory mechanisms within the same pathway to overcome drug pressure on cancer cells. The combinatory application of targeted therapy and immunotherapy is currently in the early stages of clinical studies [43].

Immune checkpoint inhibitors (ICIs)

T cells play a central role in cancer immunity. They are activated by antigen-presenting dendritic cells which leads to T cell migration and tumor infiltration. This process is accompanied by co-stimulatory factors like CD28/B7, CD40L/CD40, and IL2. However, excessive activation can lead to autoimmune diseases. To prevent this immoderate activation, co-inhibitory factors like CTLA-4/B7 and PD-L1/PD-1 suppress T cell activation. These circuits of checkpoint factors control immunity.

The most prominent approach to activate antitumor immunity is the targeting of the immune checkpoints (Fig.6) [44-45,109]. The breakthrough in cancer treatment came with the discovery of PD-1 upregulation during induction of T cell death. PD-1 is expressed in B and T cells while its ligand, PD-1L, is present on other immune and non-immune cells including cancer cells. The expression of PD-1L on cancer cells and its binding to PD-1 suppress T cells attack [46]. This feature was exploited to produce immune checkpoint inhibitors against PD-1 and its ligand to prevent their interactions [47–49]. Blocking this interaction can stimulate an antitumor response in NSCLC patients with so-called “hot-tumors” which are characterised by increased PD-L1 expression and accumulation of CD8+ tumor-infiltrating lymphocytes [36]. In KRAS LUAC, the PD-L1 is highly expressed and anti-PD-1/PD-L1 therapy was already approved [50]. However, not all KRAS patients benefit from anti-PD-1 therapy since there is a difference in efficacy among KRAS-mutant subtypes [51].

Another target of immune checkpoints is CTLA-4. Rather than participating in T cell activation, it transmits an inhibitory signal to antigen-presenting cells playing an

important role in maintaining immune tolerance. However, the anti-CTLA-4 inhibitors failed to provide encouraging results in NSCLC patients with EGFR mutations [38,50].

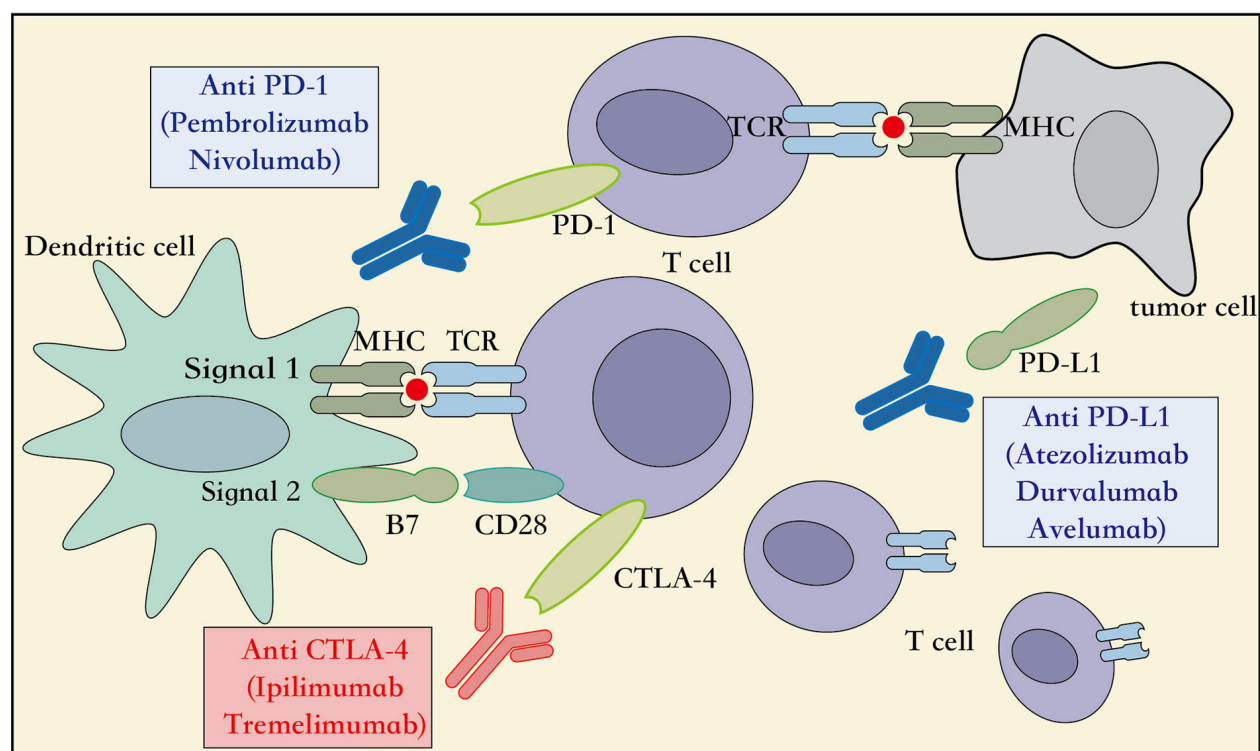


Figure 6. Regulatory mechanism of immune checkpoint inhibitors (ICI). Stimulatory and inhibitory factors control cancer-immune cycle. CTLA-4, cytotoxic T lymphocyte associated protein 4; PD-1, programmed cell death 1; PD-L1, programmed cell death ligand 1. ICIs bind to PD-1, PD-L1 or CTLA-4 allowing T cells to kill tumor cells. Adapted from [109].

Combined therapies

Although ICIs used as monotherapy did not provide a universal advantage for cancer patients, the combination of inhibitors may change this outlook. The combination of CTLA-4 (ipilimumab) and PD-L1 (nivolumab) inhibitors showed greater tumor regression in melanoma patients compared to the usage of a single drug alone [52]. In regard to lung cancer, several clinical studies using combined immunotherapy are ongoing.

The treatment of lung cancer with a combination of immuno- and chemotherapy may show a synergistic effect too. Application of chemotherapy was shown to influence the immune response via autophagy induction and ATP release in tumor cells as well as activation of NK cells to prevent immunosuppression [53,54]. As with combined immunotherapy, there are currently clinical studies using concurrent ICI and chemotherapy in progress.

Radiation has been also seen as immunogenic and could therefore prompt an immune response to promote the death of cancer cells [43]. The interplay between radiotherapy and ICIs was shown in KRAS-driven NSCLC mouse models. The application of radiotherapy drove the upregulation of PD-1 in cancer cells while simultaneous administration of anti-PD-1 inhibitor generated antitumor immunity and endured tumor control [41]. Similar results were observed in melanoma mouse models with combined anti-PD-1 immunotherapy and chemotherapy [55]. However, comparable clinical studies for human patients still need to be realised.

Sphingosine kinase I and cancer

Many biochemical processes happening in the cell are driven by a specific class of enzymes called kinases. Kinases transfer phosphate groups to certain substrates like proteins, lipids, and carbohydrates, leading to either their activation or inhibition. One of the kinases that phosphorylate lipid substrates is a sphingosine kinase 1 (SK1), a key member of the pleiotropic sphingolipids signalling pathway which was shown to be involved in tumorigenesis via phosphorylation and activation of sphingosine-1-phosphate (S1P) [56].

Multifactorial role of sphingosine-1-phosphate

Sphingolipids are essential structural lipids found in membranes of all eukaryotic cells and are involved in pathways regulating cell survival, proliferation, and apoptosis [57]. The most prominent bioactive lipids are ceramide, sphingosine, and its derivative S1P, with the latter being the most studied sphingolipid [58]. The ceramide is structurally the simplest form of sphingolipids which can be reversely converted to sphingosine by ceramidase and ceramide synthase. In turn, generated sphingosine is also reversely converted to S1P by sphingosine kinases 1/2 and sphingosine phosphate phosphatase. The cleavage by S1P lyases is the only exit point of the S1P metabolism pathway.

While ceramide and sphingosine are involved in anti-proliferation signalling, the S1P plays a role in pro-survival pathways. Due to their opposing roles in cell fate, the interplay between ceramide, sphingosine, and S1P is called a cellular rheostat which maintains an equilibrium between the cell death and its survival [59]. Thus, under normal physiological conditions, the concentration of these lipids in the cell is tightly controlled as well as the enzymes involved in sphingolipids' metabolism (Fig. 7) [60,61].

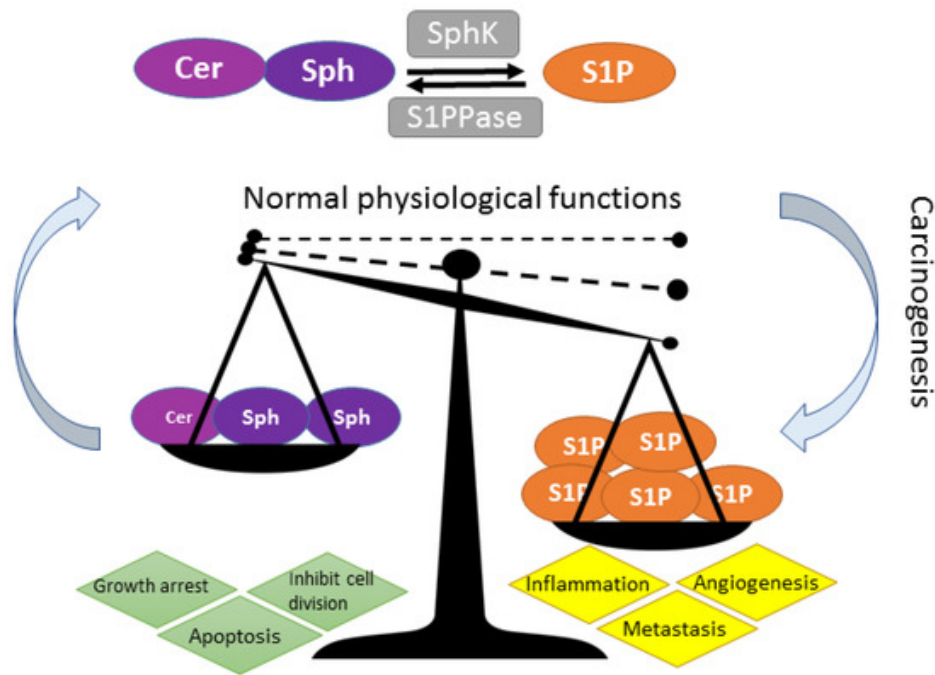


Figure 7. SK-S1P rheostat. Cer, ceramide; Sph, sphingosine; SphK, sphingosine kinase, S1P, sphingosine-1-phosphate. Regulation of S1P is dependent on SK1 (SphK). Overproduction of S1P from sphingosine leads to misregulation of cellular processes leading to carcinogenesis. Adapted from [108].

S1P is vital for the cell in terms that it can signal both intracellularly and extracellularly and it regulates various physiological and pathological processes including proliferation, apoptosis, cell migration, calcium homeostasis, angiogenesis, and vascular maturation [62,63]. S1P can be released from the cell and act in an autocrine or paracrine manner via binding to one of five G-protein coupled receptors (GPCR) called S1PRs. This binding leads to activation of canonical GPCR signalling pathways such as MAPK, PI3K, Rho, NF- κ B, and JAK/STAT pathways [64]. Intracellularly, the S1P action is less studied but is known for apoptosis protection, cell growth, and calcium homeostasis [65]. The misregulation of S1P has been shown to promote inflammation, metabolic diseases, and tumorigenesis (Fig. 7) [67,68,108].

Sphingosine kinases and S1P

The generation of S1P from sphingosine can be achieved by the action of two isozymes, SK1 and SK2. The genes of these kinases are located in different chromosomes and their products differ in amino acids length, molecular weight, and share only partial homology namely in the catalytic domain [63,65,69]. SK1 and SK2 play distinct roles in the cell. Specifically, SK1 is involved in the proliferation and survival of the cell, whereas SK2 was shown to enhance apoptosis [70]. This is supported by the

studies elucidating localization of the kinases in the cell and tissues distribution. SK1 is highly expressed in the spleen, lungs, and leukocytes and predominantly localised to the plasma membrane and the cytosol, whereas SK2 is highly expressed in the kidney and liver and mostly restricted to the nucleus, mitochondria, and ER [71]. The analysis of tissue biopsies from cancer patients showed the overexpression of SK1, particularly in breast, colon, prostate, and lung cancers [72–74]. Thus, the SK1 was subjected to numerous studies to elucidate its role in tumorigenesis.

Sphingosine kinases 1 and cancer

The initial hint that SK1 might play a role in tumorigenesis came from *in vitro* studies where overexpression of SK1 led to decreased apoptosis and enhanced proliferation in various cell lines [75]. Later, the studies on patients with breast cancer revealed that in 62,6% of tumors there was a 2-fold increase of SK1 mRNA expression level compared to healthy surrounding tissue [76]. Moreover, triple-negative breast cancer, which is considered the most aggressive type of breast cancer with metastatic potential, exhibited the highest SK1 expression with a worse prognosis and overall outcome. This poor outcome was due to the resistance to doxorubicin and docetaxel-based chemotherapies which are the approved therapies against estrogen receptor type breast cancer. Studies on 48 patients with glioblastomas revealed that the median survival time of the patients with higher SK1 expression was 102 days while patients with lower SK1 had a 3-fold increase in median survival time [77]. Additionally, SK1 but not SK2 was shown to be responsible for the secretion of S1P out of breast cancer cells which led to lymphangiogenesis and lymph node metastasis [78,79].

The role of SK1 in the tumor microenvironment of pancreatic cancer was elucidated in a mouse model. The bioluminescent imaging showed a reduced tumor burden after panc02-luc murine pancreatic cancer cells (with intact SK1) were injected into mice lacking SK1 [80,81]. Further, there were fewer infiltrating lymphocytes around and within tumors in SK1 deficient mice compared to wild type. In addition, this study demonstrated that host SK1 contributed to the proliferation of injected cancer cells via the S1P axis and the recruitment of lymphocytes to the pancreatic tumors. Another group showed that SK1 promotes drug resistance in pancreatic cancer peritoneal carcinomatosis. Using cytotoxic assay with gemcitabine, the drug used in pancreatic cancer treatment, they showed that SK1 deficient cells were less viable after drug

administration compared to non-treatable cells [82]. SK1 also contributed to resistance against the most promising ICI treatment in *in vitro* melanoma models [83].

In regard to the NSCLC lung cancer patients, SK1 mRNA level along with its protein level was significantly higher in tumor cells compared to the surrounding healthy tissue leading to a poor overall prognosis. As well as in pancreatic cancer, SK1 overexpression promoted significant resistance to doxorubicin- or docetaxel-induced apoptosis via activation of PI3K/Akt/NF- κ B pathway and antiapoptotic proteins like TRAF2 and Bcl-xl [84]. Immunohistochemical analysis of 176 NSCLC patient samples showed highly elevated SK1 levels in adenocarcinomas compared to surrounding stroma. This significant SK1 overexpression was associated with the advanced clinical stage of the disease and as a consequence with the shorter survival. Moreover, this study demonstrated that high SK1 levels led to cancer relapse in NSCLC patients treated with adjuvant chemotherapy [85].

Sphingosine kinases 1 inhibitors

The recognition of the importance of SK1 in cancer led to development of numerous SK1 inhibitory compounds. These compounds can bind to sphingosine or ATP pockets of SK1 or associate with SK1 substrates. Initial inhibitors displayed limited specificity. In particular, this was a case of structural-based analogs of sphingosine. Later studies identified several SK1 inhibitors (like SK1-I, SK1-II, PF-543, compound 11, SKI-349, MP-A08, ABC294640) with higher affinity, greater specificity and antitumor activity [70]. However, some of these compounds exhibited dual SK1/SK2 activity. SK1-I is a SK1-specific inhibitor which was shown to reduce proliferation and survival of Jurkat and human leukemias U937 cells [84]. SK-II induced lysosomal degradation of SK1 [85] and decreased S1P production in mouse mammary adenocarcinoma cells [70]. However, in another study it was shown to act against both SK1 and SK2 [86]. The compound-11g is the most potent SK1 inhibitor reported today [87].

Aims of this study

Regardless of the recent progress in the treatment of lung cancer patients (particularly NSCLCs), the overall survival of these patients remains ~ 15% only [83]. This is due to the development of drug resistance of cancer cells. Many cancer cells use alternative signalling pathways and specific mutations to overcome the treatment and immune pressure. Recently, the focus of the scientific community has shifted from protein-based to lipid-based targets, especially sphingolipids, as a promising tool in cancer treatment [88]. This is the case with SK1. As SK1 drives the formation of S1P and indirectly blocks ceramide production via clearances of sphingosine, it is considered a key enzyme in the regulation of bioactive sphingolipids levels [60]. Although SK2 can produce S1P, the inhibition or degradation of SK1 could prevent alteration of cellular S1P balance, thus preventing S1P from following the pro-survival signalling pathway.

Combination of treatments was proposed to reduce the tumor resistance. To explore this possibility, our lab conducted afatinib-based high-throughput synergism analyses in KRAS mutated LUAD of both human and mouse origin. This allowed us identification of afatinib-based drug combinations which could potentially boost efficacy of afatinib in KRAS-driven LUAD. Interestingly, along several others, SK1 was the most promising target in combination with afatinib administration. Hence, the general goal of this study was to elucidate the role of the SK1 in the growth, survival, and potential oncogenic signalling pathways of tumor cells. For this, we generated the SK1 knock-out cell line in KRAS mutated mouse tumor cells via the CRISPR/Cas9 system. These cells were characterised and analysed through various functional tests to describe their proliferation and migration capacity. To assess the KO cell lines' migration patterns, wound healing assays was performed. For this, we generated GFP expressing lentiviruses to produce control and KO cell lines expressing GFP protein. Since SK1 also regulates NF- κ B activity, we assessed possible alterations in the cellular inflammatory response (PD-I1, STAT 1, *etc*) upon pro-inflammatory stimulation with TNF α and IFN γ .

Materials and Methods

Mammalian cell lines

In this study, we used murine lung adenocarcinoma cells. These cells were previously isolated from lung adenocarcinoma of KRAS^{LSL-G12D} p53^{fl/fl} mice harbouring an oncogenic point mutation in G12D KRAS allele. The expression of this allele was prevented by the Lox-Stop-Lox cassette located upstream of the transcriptional start site. The inhalation with adenovirus-expressing Cre-recombinase triggered activation of KRAS^{G12D} and deletion of p53 alleles in lung epithelial cells leading to the development of adenocarcinomas [87]. Cells were further called KP cells.

Cell culturing medium

The RPMI-1640 (Sigma-Aldrich) medium containing L-glutamine and sodium bicarbonate was supplemented with 10% foetal bovine serum (FBS) (Capricorn Scientific GmbH) and 1% Penicillin-Streptomycin (Sigma-Aldrich) (further called complete medium). Cells were cultured at 37 °C in an incubator with 5% CO₂. For cell detachment, Trypsin-EDTA solution (Sigma-Aldrich) diluted in 1x PBS in a ratio of 3:1 was used. Cells were briefly washed with warm 1x PBS to remove dead cells. Two-three ml of Trypsin-EDTA-PBS solution was added and cells were incubated for no more than 5 min in a CO₂ incubator. After detachment, cells were resuspended with a 1ml pipette tip and 1/10 of the total cell number were transferred to a new 10cm Petri dish (SARSTEDT AG&Co. KG) with a fresh culture medium for culturing.

Freezing cells

Freezing medium for cell storage was prepared from RPMI-1640 medium and supplemented with 30% FBS and 10% DMSO as a cryopreserved (Cryo medium). For stock production, the cells in the exponential growth phase were used. Cells were cultured in either 175 cm² flasks (BD Falcon™ or CELLSTAR®) or in 15 cm Petri dishes and harvested at about 80-90% confluency. The pellet was resuspended in cryo medium and 1ml was aliquoted to cryovials and stored for 7-10 days in -80 °C. Afterward, cryovials were moved to liquid nitrogen for long-term storage.

Thawing cells from liquid nitrogen stock

For experiments, cells were quickly thawed at 37°C and transferred to a 15ml Falcon tube containing 10ml of complete medium. Cells were further centrifuged for 3min at 250 rcf and the pellet was resuspended and moved to a 10 cm Petri dish containing 10ml of fresh complete medium.

Counting cells

Cells were harvested and a small aliquot was 1:1 diluted with Trypan blue (Sigma-Aldrich) and counted with the DeNovix CellDrop™ cell counter. For experiments, only live cell numbers were used.

Transfection

One day before transfection the needed cells were plated either into 15 cm Petri dishes or 12-well plates. Transfection was performed using Lipofectamine 2000 (Invitrogen) and RPMI medium supplemented with 1% FBS (further reduced medium). For this, plasmid of interest (~ 500 to 1500 ng) and the lipofectamine 2000 (~2-10 µl) were added to two 1.5 ml eppendorfs containing 100 µl of reduced medium and then mixed together following 20 min incubation. The cell medium was changed to a reduced medium and transfection mix was added in a drop wise fashion. After 2-3 h, the medium was changed to complete medium, and cells were overnight incubated in a CO₂ incubator at 37°C.

Lentivirus generation

Lentiviruses expressing GFP protein were produced using a 3rd generation lentiviral system, which includes pAB64-GFP-pLenti-Puro, psPAX2, pMD2G plasmids (Addgene), and Lenti-x™ 293T cell line (Takara). The plasmids were generated using Stbl3 bacterial strain and purified using midi prep (QIAGEN® Plasmid Midi Kit). All plasmids and cell lines were in long possession of Dr. Casanova's lab.

The 5 x10⁶ Lenti-x™ 293T cells were plated in 150 mm Petri dishes with 15 ml complete media and incubated overnight at 37°C and 5% CO₂. For transfection, 1.5 µg pAB64-GFP-pLenti-Puro, 1 µg psPAX2, and 300 ng pMD2G were mixed in 100 µl of RPMI medium supplemented with 1% FBS (reduced medium). Separately, 10 µl of Lipofectamine 2000 was added to 100 µl reduced medium and in 5 min was mixed with prepared plasmids' mix. The cell medium was changed to the reduced medium and the

transfection cocktail was added to the cells. After incubation for 2-3 h, the transfection medium was substituted with a 10ml RPMI medium with 10% FBS, and cells were incubated overnight at 37°C and 5% CO₂. The next day, transfection efficiency was checked under a Nikon microscope to visually observe GFP-expressing cells. In 48h post-transfection, the supernatant was passed through a 0.45 µm sterile syringe filter (Millipore) and collected into a 50 ml Falcon tube. To concentrate the virus, 3.3 ml of 40% PEG-6000 solution in 1x PBS was added to the viral mixture and kept at + 4°C overnight. The fresh complete medium was added to the Petri dish and cells were further incubated in a CO₂ incubator at 37°C. The same procedure was performed for the next two days aiming to collect most of the viral particles for future concentration. After several days of supernatant collection, the tube was incubated on constant rocking overnight and then centrifuged at 4500 rpm for 15 min. The pellet was resuspended in 5 ml of reduced medium and either immediately used or stored at - 80°C.

Bacterial cell lines

For this study, we used DH5α and Stbl3 bacterial strains

Competent cells preparation

A single colony of bacterial DH5α and Stbl3 strains were overnight cultured in 5 ml LB medium at 37°C (DH5α) and at 30°C (Stbl3). The next day cells were diluted at 1:100 in 200 ml LB and incubated in a 1 L flask at 37°C at constant rotation until OD₆₀₀ reached 0.2 - 0.5. The cells were aliquoted to 50 ml Falcons and incubated on ice for 10 min. Afterward, cells were centrifuged for 10 min at 3000 rpm and 4°C, the pellet was resuspended in 5 ml TSS buffer and cells were aliquoted to 1.5 ml eppendorfs and frozen in liquid nitrogen (<https://openwetware.org/wiki/>).

Transformation and plasmid isolation

The competent cells were thawed on ice. The plasmid (~100-200 µg) was added, carefully mixed, and incubated on ice for 20 min. Cells were heat-shocked at 42°C for 30 sec and put back on the ice for 2 min. One ml of LB medium was added to the cells following 30 min incubation at 37°C at constant rotation. Cells were spread onto LB agar medium in 10 cm Petri dishes and incubated at 37°C overnight. The next day 2-3 single colonies were taken and bacteria were grown in 5 ml LB medium supplemented with 100 µg/ml ampicillin. Plasmids were isolated using the NucleoSpin

Plasmid Kit (Macherey-Nagel). Briefly, cells were centrifuged at 5000 rpm for 3 minutes, the supernatant discarded, and the pellet was resuspended in a resuspension buffer with RNase I. Thereafter, the pellet was lysed for 5 min with 250 µl of lysis buffer, neutralised with 300 µl of neutralisation buffer, and spun down for 10 minutes at 11000 rpm. The supernatant was carefully transferred into the NucleoSpin® column and centrifuged for 1 minute at 11000 rpm. The column was twice washed with a washing buffer following empty column centrifugation for complete ethanol removal. Next, 40 µl of elution buffer were added to the center of the column, incubated for 2 minutes, and briefly centrifuged at 11000 rpm.

For lentiviral plasmid preparation, the midiprep QIAGEN® Plasmid Midi Kit was used. Briefly, 5 ml of overnight Stbl3 cell culture bearing plasmids of interest was diluted in 100 ml of LB/ampicillin medium and incubated on rotation at 37°C for 3 h. Cells were aliquoted to two 50 ml Falcon tubes, set aside on ice for 10 min, and centrifuged at 6000 g for 6 minutes. The pellet was resuspended in 4 ml resuspension buffer and 4 ml lysis buffer was added to lyse bacterial cells. After 5 min, the reaction was neutralized with a 4 ml neutralisation buffer, incubated on ice for 15 min, and then centrifuged at 15000 g for 10 minutes at 4°C. The QIAGEN-tips were equilibrated with a 4 ml equilibration buffer and the columns were allowed to empty by flow gravity. The supernatant was added to columns and allowed to enter the resin by gravity flow. Next, the columns were washed twice with 10 ml washing buffer, and DNA was eluted with 5 ml of elution buffer. The DNA was precipitated with 3.5 ml of isopropanol and centrifuged at 15000 g for 30 minutes. The pellet was washed twice with 70 % ethanol, centrifuged at 15000 g for 10 minutes, and air-dried for 10 min. The pellet was resuspended in 100 µl TE buffer and the concentration was measured via Tecan plate reader.

CRISPR-Cas9 knock-out of Sphingosine kinase 1 gene

Preparation of guide RNA

Single guide RNA (sgRNA) for SK1 knock-out was designed using a freely available online tool (<http://crispor.tefor.net>), aiming to target exon 2 of the SK1 gene. It was introduced into Cas9 expressing vector with puromycin resistance gene pSpCas9(BB)-2A-Puro (PX459) V2.0 (Addgene) as previously described in [90]. For this, 5' restriction sites for BbsI restrictase was added to the oligonucleotides. Afterward, the 5' ends of the top and bottom sgRNA oligonucleotides were phosphorylated for 30

minutes and annealed at 95°C for 5 min following a slow drop in temperature until 22°C (Table 1 and Table 2).

Guide RNA	Sequence	Name of the clone
Mus musculus mSK1	top 5' CACCGCATCTGTTCTACGTACGTG	KP ^Δ SK1
	bottom 5' AAACCACGTACGTAGAACAGATGC	

Table 1. SgRNA sequences. SgRNA was designed to target exon 2 of *mus musculus* SK1.

Phosphorylation and annealing reaction mix	Amount
ddH ₂ O	6 µl
sgRNA top (100 µM)	1 µl
sgRNA bottom (100 µM)	1 µl
T4 ligation buffer (10X)	1 µl
T4 PNK	1 µl

Table 2. Phosphorylation and annealing of sgRNAs reaction mix.

The reaction mix was further diluted at 1:200 in ddH₂O, cloned into pSpCas9(BB)-2A-Puro with incubation at room temperature for 1 h. The reaction mix lacking duplex oligonucleotide was used as a negative control (Table 3).

Reaction mix	Amount
ddH ₂ O	13.5 µl
Diluted oligonucleotide duplex	2 µl
pSpCas9(BB)-2A-Puro (PX459) V2.0 (100ng/µl)	1 µl
FastDigest BbsI	1 µl
T4 Ligation buffer	2 µl
T4 ligase	0.5 µl

Table 3. Cloning of annealed sgRNAs into pSCas9(BB)-2A-Puro vector.

The transformation was performed in DH5α competent cells according to the previously described protocol. Cells were plated into LB agar medium containing 100 µg/ml ampicillin and incubated at 37°C overnight. Next, 3 single colonies were isolated and cultured overnight in 5 ml LB-ampicillin medium following plasmid isolation.

Plasmids were digested with BbsI restriction enzymes to confirm the presence of the insert and afterwards sent for sequencing using universal U6-Fwd primer.

Generation of pools

To generate pools lacking SK1, 1×10^5 KP cells were plated into each well of 12-well plate following next day transfection as described above. For transfection, 500 ng of each plasmid were used. As a control for successful transformation, we utilised pSpCas9(BB)-2A-GFP (Addgene) plasmid lacking the puromycin resistance gene. In 24 h, cells were checked for the presence of fluorescently labeled cells in the control well. For clonal selection, 4 μ g of puromycin were applied based on previous titration and cells were cultured in a CO₂ incubator at 37°C for three days. Afterward, wells were washed with 1x PBS and complete media was added. Once surviving cells reached ~80% confluency, they were trypsinized and moved to a 6-well plate for expansion. Then, cells were split into two parts: one part was used for DNA analysis while another part was frozen.

DNA isolation

To isolate DNA, cells were centrifuged at 2000 rpm, and the pellet was lysed in 200 μ l lysis buffer with 30 μ g/ml of Proteinase K (Sigma Aldrich) overnight (Table 4). The next day, 85 μ l of 5 M NaCl were added to the lysed cells and centrifuged for 10 minutes at 16000 rpm. The supernatant was transferred to a new eppendorf tube, 200 μ l of isopropanol (Roth) was added, briefly mixed, and centrifuged for 5 min at 16000 rpm. After centrifugation, the isopropanol was carefully removed and 1 ml of 70 % ethanol was added. The mix was centrifuged for 10 minutes at the same speed, the supernatant was discarded, and the pellet was air-dried for 30 minutes. Once the remaining ethanol evaporated, the pellet was resuspended in 20 μ l of nuclease-free water. The concentration was determined using a Tecan plate reader.

Reagent	Concentration
Tris-HCL pH 8	50 mM
EDTA	100 mM
NaCL	100 mM
SDS	1 %

Table 4. Composition of DNA lysis buffer.

PCR amplification

To confirm the presence of knock-out, PCR with corresponding primers targeting a specific region of the putative nick was performed (Table 5). Therefore, 500 ng of purified DNA with putative knock-out was used for amplification in the reaction mixture (Table 6). DNA from KP parental cells served as a control.

Primer name	5' - 3' sequence
mSK1 - fwd - TIDE	TTTGTTGCTGACGTGGACCT
mSK1 - rev - TIDE	CATCCACAGAAAACACGCC

Table 5. TIDE primers.

Reagents	Amount	Temperature	Time
ddH ₂ O	32.5 µl	94°C	2 min
GoTaq Buffer 10x	10 µl	94°C	30 sec
Primer fwd and rev mix (10 mM)	2 µl	59°C	40 sec
dNTPs (5µM)	2 µl	72°C	50 sec
DNA (500ng)	3 µl	72°C	10 min
GoTaq Polymerase	0.5 µl	4°C	∞

Table 6. Reaction mixture for amplification of SK1 targeting sequence.

Agarose gel electrophoresis

To visualise the amplification of PCR products, 1.5 % agarose gel was prepared. Briefly, 1.5 g of agarose (Sigma Aldrich) was dissolved in 120 ml 1x TAE buffer, and 2 µl of Sybr® Safe DNA gel dye (Thermo Scientific) was added. The agarose solution was cast in a transparent tray with a comb and allowed to solidify for ~ 20 min. The 5µl of amplified PCR products along with a 5µl GeneRuler 1 kbp (ThermoFisher) were loaded into the gel, run for 30 minutes at 100 V, and visualised under UV light in the ChemiDoc™ XRS (Bio-Rad).

Purification of PCR fragments

Once the presence of amplified fragments was detected, the PCR product was purified using FavorPrep™ PCR Clean-Up Mini Kit (Favorgen). Briefly, the PCR mix was

mixed with 250µl of FADF buffer, transferred to the FADF column, and centrifuged for 1 minute at 13000 rpm. The supernatant was discarded, 500 µl of washing buffer containing ethanol was added, centrifuged for 1 minute at 13000 rpm. The supernatant was again removed and the column was centrifuged for 3 minutes at 10000 rpm. The purified PCR product was eluted by adding 20 µl of elution buffer to the center of the column, incubated at room temperature for 3 minutes, and centrifuged again. The concentration of eluted PCR product was determined using a Tecan plate reader.

Sequencing of PCR product

To check the presence of knock-out, 10 µl (~100 ng) of the purified PCR product with 5 µl of forward primer, which was used in the PCR amplification mix, were sent for sequencing. The obtained results were analysed using a free online tool, Tide (<https://tide.nki.nl>). If more than 65% of cells in the pool contained the targeted mutation (detected indels), the pool was considered for single clones production.

Generation of single clones

To prepare single clones from pools containing the targeted mutation, cells were subjected to limited dilution titration. For this, the putative pool was thawed and allowed to grow for 1-2 days. After recovery from deep freezing, cells were trypsinized and counted. The specific amount of medium containing 50 cells was added to 10 ml of complete medium, thoroughly mixed and 100 µl of the mixed medium was added to each well of a 96-well plate. Cells were growing for ~14 days and the presence of expanded colonies was confirmed under the light microscope. Next, the single colonies were transferred to the 12-well plate and allowed to expand until ~90 % confluency. Once the desired confluence was reached, cells were harvested and divided into two parts: one part was subjected to DNA isolation, the other part- for deep freezing. All the remaining steps such as DNA isolation, PCR amplification, and TIDE analysis were performed according to previously described protocols.

Real-time PCR

RNA extraction

The E.Z.N.A.® Total RNA Kit I (Omega Bio-tek, Inc.) was used to isolate total RNA from KP and KP^{ΔSK1} cells. Briefly, 1 x10⁵ cells were seeded in a 12-well plate, and

in 24 h cells were lysed with 350 μ l lysis buffer and stored at -20°C . Prior to RNA isolation, the cell lysates were thawed on ice, collected into homogeniser minicolumns, and centrifuged for 2 min at 12,000 x g. The homogenized lysates were transferred into fresh 1.5 ml eppendorfs and 1 volume of 70 % ethanol was added. The lysate mixtures were afterward transferred into preassembled HiBind® RNA Mini Columns and centrifuged for 1 minute at 10,000 x g. The columns were washed twice with the washing buffer, centrifuged for 1 minute at 10,000 x g, and RNA was eluted with 40 μ l nuclease-free water and stored at -20°C .

Reverse transcriptase-PCR (RT-PCR)

To convert the total RNA to cDNA, the iScript™ cDNA synthesis kit (Bio-Rad) was used. At first, the total RNA was quantified at the Tecan plate reader and 400 ng of each RNA sample was converted to cDNA according to Table 7A and 7B. The cDNA was stored at -20°C .

Reagents	Volume
ddH ₂ O	to 20 μ l
5x iScript reaction mix	4 μ l
RNA sample (400 ng)	varies
iScript reverse transcriptase	1 μ l

Table 7A. Reaction mixture for amplification of SK1 targeting sequence.

Thermocycler program	Time and temperature
Priming	5 min at 25°C
Reverse transcription	20 min at 46°C
RT inactivation	1 min at 95°C

Table 7B. Reaction mixture for amplification of SK1 targeting sequence.

Quantitative real-time PCR (qPCR)

Prior to qPCR reaction, the cDNA was diluted at 1:25 in NFW and the qPCR reaction mix was assembled according to Bio-Rad iTaq Universal SYBR® Green Supermix (Table 8A and 8B). The qPCR primers were designed using the Primer-blast

tool (<https://www.ncbi.nlm.nih.gov/>) (Table 9) and normalised to threshold cycles of 28S RNA to calculate relative differences in gene expression profile.

qPCR reaction mix	Volume
ddH ₂ O	1.75 µl
Forward qPCR primer (10 µlM)	0.375 µl
Reverse qPCR primer (10 µlM)	0.375 µl
iTaq™ Universal SYBR® Green Supermix (Bio-Rad)	7.5 µl
Diluted 1:25 cDNA	5 µl

Table 8A. Reaction mixture for qPCR.

qPCR program	Time	Cycles
initial denaturation at 95°C	30s	
95°C	5s	2 x 40
60°C	30s	
65°C	5s	
95°C	5s	

Table 8B. Amplification condition of qPCR.

Primer name	5' - 3' sequence
<i>Sphk1</i> - fwd	TCCTTCAACCTCATACAGACAG
<i>Sphk1</i> - rev	ATTCAGCACCTCGTAAAGCAG
<i>Fascin1</i> - fwd	CCACTGCGTCCACCAAGAAC
<i>Fascin1</i> - rev	GGTCACAAACTTGCCGTTGG
28s - fwd	ATACCGGCACGAGACCGATAGTCA
28s- rev	GCGGACCCACCCGTTTACCTC
<i>Ctnnb1</i>- fwd	CACAGCTCCTTCCCTGAGTG
<i>Ctnnb1</i>- rev	ACTGCCCGTCAATATCAGCTAC
<i>Cdh1</i>- fwd	CAGAGTTTACCCAGCCGGTC
<i>Cdh1</i>- rev	CTTCATCACGGAGGTTCTCTGG
<i>Cdh2</i>- fwd	GGCTGAAAATAGACCCCGTG
<i>Cdh2</i>- rev	TCATAGGCGGGATTCCATTGTC
<i>Snail1</i>- fwd	GGAGTTGACTACCGACCTTGC
<i>Snail1</i>- rev	GCTGGAAGGTGAACTCCACAC
<i>Snail2</i>- fwd	CACATTAGAACTCACACTGGGG
<i>Snail2</i>- rev	TGCCCTCAGGTTTGATCTGTC
<i>Vim</i>- fwd	GCGAGGAGAGCAGGATTTCTC
<i>Vim</i>- rev	GTCCATCTCTGGTCTCAACCG
<i>Cd274</i>- fwd	AACGCCACAGCGAATGATG
<i>Cd274</i>- rev	ATGTGTTGCAGGCAGTTCTGG
<i>Hif1a</i>- fwd	ATGCTCTCACTCTGCTGGC
<i>Hif1a</i>- rev	ATGCTCTCACTCTGCTGGC
<i>Ctla4</i>- fwd	TGGGTTTTACTCTGCTCCCTG
<i>Ctla4</i>- rev	GTTGGGTCACCTGTATGGCTTC

Table 9. RT-qPCR primer sequences.

Western blotting

Cells preparation for protein isolation

To test the expression of the proteins of interest, 5×10^5 cells were plated in a 6-well plate 24 h before isolation. The next day, cells were twice washed with 1x PBS, stimulated with 5 ng/ml IFN γ for 15 minutes and/or with TNF α for 4 h, and quickly lysed with 80 μ l ice-cold lysis buffer (Table 10). Cells were scraped with the scraper on ice, the lysates were transferred into 1.5 ml cold eppendorfs, and frozen at - 80°C. On a third day, the lysates were centrifuged for 15 min at 4°C and supernatant was taken for BCA assay.

Reagent	Final concentration	Amount to add to 50 ml
1 M Tris pH 7.5	20 mM	1 ml
5 M NaCl	100 mM	1 ml
100 mM Na ₃ VO ₄	1 mM	0.5 ml
500 mM NaF	100 mM	10 ml
200 mM Glycerol-2-phosphate	20 mM	5 ml
250 mM EDTA	2.4 mM	0.5 ml
250 mM EGTA	1 mM	0.2 ml
NP-40	1 %	0.5 ml
Protease inhibitor cocktail		5 tabs

Table 10. Lysis buffer for cells.

BCA assay

BCA assay was used to determine protein concentrations. The bovine serum albumin (BSA) standards were prepared according to BioVision protocol from 1 μ g/ μ l BSA stock. The 2.5 μ l of protein solution (on ice) was diluted with 22.5 μ l of ice-cold lysis buffer and 200 μ l of BSA standards (2000 ng, 1500 ng, 1000 ng, 500 ng, 250 ng, 125 ng, 25 ng, 0 ng) were added to the protein mix in duplicates in 96-well plate. The plate was incubated at 37°C for 30 min and the absorbance 562 nm was measured via Tecan plate reader. The standard curve was plotted following the calculations of protein concentrations.

Samples preparations and SDS-PAGE

Based on the results of the Bradford assay, samples were prepared at final concentrations of 20 µg and diluted in a 6x Laemmli buffer (Table 11). The 10x running buffer for SDS-PAGE gels were prepared according to the Boston-Bio-Products protocol (Table 12). To prepare gel, 5.5 ml of 10 % resolving gel solution (Table 13) was poured into assembled 1 mm glass plates and covered with 40 µl isopropanol to allow polymerisation. Once the gel polymerised, isopropanol was removed, 2 ml of stacking gel solution (Table 14) was added, and the 15-well comb was placed. After complete polymerisation, the comb was removed, the gel was washed with ddH₂O to remove the remaining SDS, and the plates were assembled into an electrode chamber. The samples were heated for 3 minutes at 95°C and loaded into the gel along with 3 µl of Precision Plus Protein™ Standards (Bio-Rad) and run in the 1x running buffer. The gels were first to run for 20 min at 80 V and afterwards at 130 V until the lower proteins reached the glass plate border.

Reagents	Final concentration	Amount to add to 10 ml
1 M Tris base	375 mM	3.75 ml
10 % SDS	9 %	0.9 ml
99 % Glycerol	50 %	5 ml
Beta-mercaptoethanol	9 %	0.9 ml
Bromphenol blue	0,03 %	0.03 ml

Table 11. Composition of 6x Laemmli buffer.

Reagents	Amount to add to 1L
0.25 M Tris base	30.29 g
1.92 M Glycine	144.13 g
1 % SDS	10 g
pH 8.3	

Table 12. Composition of 10 xRunning buffer, pH 8.3.

Reagents	Volume (10 ml)
ddH ₂ O	4 ml
30 % Bis-acrylamid	3.3 ml
1.5 M tris-Cl pH 8.8	2.5 ml
10 % SDS	0.1 ml
10 % APS	0.1 ml
TEMED	0.004 ml

Table 13. Composition of 10 % resolving gel solution.

Reagents	Volume (2 .5 ml)
ddH ₂ O	1.7 ml
30 % Bis-acrylamid	0.415 ml
1 M tris-Cl pH 6.8	0.315 ml
10 % SDS	0.025 ml
10 % APS	0.025 ml
TEMED	0.0025 ml

Table 14. Composition of 5 % stacking gel solution.

Semi-dry transfer

To transfer proteins from gels to either 0.45 nitrocellulose or PVDF membranes (AmershamTM, GE Healthcare Life Science), the semi-dry system was used. The membrane and filter papers were briefly incubated in the transfer buffer (Table 15), and the sandwich was assembled according to Trans-Blot® SD cell protocol (Bio-Rad). The transfer was performed for 1 h at a constant 80 mA per membrane.

Reagents	Amount to add to 1L
0.48 M Tris base	58.16 g
0.39 M Glycine	29.28 g
0.375 % SDS	3.75 g
add 1:10 methanol before usage	

Table 15. Composition of 10x semi-dry transfer buffer.

Antibody detection

To confirm the successful transfer, the membrane was briefly washed with ddH₂O, incubated for 5 minutes at constant rocking with Ponceau Red solution, and imaged in ChemiDoc™ Imaging System (Biorad) . Then, the membranes were three times washed with ddH₂O and incubated with PBST+5 % milk (1x PBS, 0.5 % Tween 20, and 5 % skim milk) for 40 minutes to block any nonspecific sites. The antibodies were diluted at different concentrations (Table 16) in 5 ml of PBST+5 % milk solution, added to the membrane, and incubated at 4°C overnight. The next day, membranes were washed four times for 5 min each with a washing buffer (PBS and 0.05 % Tween 20) and incubated with HRP conjugated secondary antibody for 1 h at room temperature. Next, the membranes were four times washed with the washing buffer, proteins were detected using Pierce™ ECL Western Blotting Substrate (ThermoFisher) and imaged in ChemiDoc™ Imaging System (Biorad).

Antigen	Dilution	Manufacture
Mouse HSC 70	1:1000	Santa Cruz Biotechnology
Mouse SK 1	1:1000	Santa Cruz Biotechnology
Mouse Fascin 1	1:1000	Santa Cruz Biotechnology
Anti-mouse IgG, HRP-linked	1:5000	Cell Signaling

Table 16. Primary and secondary antibodies.

Cell-based assays

Cell proliferation assay

2 x 10⁵ cells in triplicates were plated into a 6-well plate (SARSTEDT AG & Co. KG) and subsequently trypsinized and counted 24h, 48h, 72h, and 96h after initial seeding.

Wound-healing assay

For this assay, 4 x 10⁵ cells in triplicates were plated into a 12-well plate aiming to reach ~90 % confluency the next day. In 24 h post-seeding, vertical and horizontal scratches were performed with a 200 µl pipette tip. The wells were washed with 1x PBS and pictures were taken immediately after, in 24 h, in 48 h, and 72 h using Nikon

inverted microscope Eclipse Ts2-FL. Quantification of the wound area was performed with an ImageJ wound healing plug-in [91].

Lentiviral transduction of KP and KP Δ SK1 cell line

To produce KP and KP Δ SK1 cell lines expressing GFP (further called KP-GFP and KP Δ SK1-GFP), 1 x10⁵ KP and KP Δ SK1 cells were plated into a 12-well plate. In 24 h 1 ml of the viral solution was added to each well. To increase the transduction efficiency, 8 μ g of Polybrene (Sigma Aldrich) was added to each well. The medium was changed one day after transduction and cells were incubated in a CO₂ incubator at 37°C for two additional days. For selection, 5 μ g of puromycin was added to the GFP-expressing cells. Cells were cultured for two weeks with a presence of 5 μ g of puromycin.

Scratch assay with fluorescently labeled cells

Fluorescently labeled KP Δ SK1-GFP and KP-GFP cells were mixed 1:1 ration and 2.5 x 10⁵ cells were plated in triplicates into a 12-well plate according to Table 17. After 24 h, cells reached ~ 90 % confluency and scratch was performed using 200 μ l pipette tip. Wells were washed with 1x PBS, covered with complete medium, and pictures were taken at 0 h, in 24 h and 48 h.

	1	2	3	4
A	KP- KP Δ SK1_GFP	KP Δ SK1-KP Δ SK1_GFP	KP- KP_GFP	KP Δ SK1 - KP_GFP
B	KP- KP Δ SK1_GFP	KP Δ SK1-KP Δ SK1_GFP	KP- KP_GFP	KP Δ SK1 - KP_GFP
C	KP- KP Δ SK1_GFP	KP Δ SK1-KP Δ SK1_GFP	KP- KP_GFP	KP Δ SK1 - KP_GFP

Table 17. Combination of fluorescently labelled KP and KP Δ SK1 cells.

Proliferation assay

To check the ability of sphingosine-1-phosphate to influence KP Δ SK1, the CellTrace™ Violet Cell Proliferation Kit and CellTrace™ CFSE Cell Proliferation Kit (Invitrogen) were used. For this, 1 x 10⁶ KP and KP Δ SK1 cells were harvested and washed twice with 1x PBS to eliminate any remaining FBS. In order to label the cells, 1

μ l of each dye was diluted in 1 ml of 1x PBS then added to cells and incubated in the dark for 15 min at 37°C. For dye inactivation, 5 ml of complete RPMI medium was added and incubated for an additional 5 min at 37°C in the dark. Next, the cells were centrifuged for 3 minutes at 300 rpm and 1 ml of complete RPMI medium was added. The cells were mixed according to Table 18.

Dye	Cell number
KP - violet	2.5 x10 ⁵
KP - CFSC	2.5 x10 ⁵
KP^{ΔSK1} - violet	2.5 x10 ⁵
KP^{ΔSK1} - CFSC	2.5 x10 ⁵
KP - violet / KP^{ΔSK1} - CFSC	2.5 x10 ⁵ / 2.5 x10 ⁵
KP - CFSC / KP^{ΔSK1} - CFSC	2.5 x10 ⁵ / 2.5 x10 ⁵

Table 18. Combination of KP and KP ^{Δ SK1} cells stained with CellTrace dyes.

After 72 h, cells were harvested, washed with 1x PBS, and subjected to the life/dead staining with BD Horizon™ Fixable Viability Stain 620. As previously mentioned, 1 μ l dye was diluted in 1x PBS, added to the cells, and the mix was incubated in the dark for 7 minutes at 37°C. The dye was inactivated with the addition of 5 ml complete RPMI medium for 5 minutes. Afterward, cells were centrifuged and the pellets were resuspended in 400 μ l of 1x PBS with 3% FBS. For FACS controls, the mixture of unstained KP and KP ^{Δ SK1} cells, as well as freshly stained cells with CellTrace™ CFSE and CellTrace™ Violet dyes, were used.

Rescue experiment

For the rescue experiment, 2.5 x 10⁵ KP and KP ^{Δ SK1} cells were plated into 6 cm Petri dishes in triplicates and cultured in a CO₂ incubator for 48 h. The supernatant of these cells was collected and filtered via a 0.40 μ m filter. New 2.5 x 10⁵ KP and KP ^{Δ SK1} cells were plated in triplicates and the filtered supernatant was added based on different conditions according to Table 19. In 72 h, cells were harvested and counted.

	KP cells	KP ^{ΔSK1} cells
Condition 1	KP control	KP ^{ΔSK1} control
Condition 2	KP + 100% KP ^{ΔSK1} supernatant + 10% FBS	KP ^{ΔSK1} + 100% KP supernatant + 10% FBS
Condition 3	KP+50% KP ^{ΔSK1} supernatant+50% RPMI+10% FBS	KP ^{ΔSK1} +50% KP supernatant+50% RPMI+10% FBS
Condition 4	KP + 100% KP supernatant + 10% FBS	KP ^{ΔSK1} + 100% KP ^{ΔSK1} supernatant + 10% FBS
Condition 5	KP + 50% KP supernatant + 50% RPMI + 10% FBS	KP ^{ΔSK1} + 50% KP ^{ΔSK1} supernatant + 50% RPMI + 10% FBS

Table 19. Combination of KP and KP^{ΔSK1} for rescue experiment.

Transwell and invasion assays

For the transwell assay, a 12 well plate with the transwell inserts was used. 600 μ l of complete RPMI medium were added into the wells and transwell inserts were put into six wells. The 3.5×10^4 KP and KP^{ΔSK1} cells per well were resuspended in the reduced medium with just 2% of FBS plated in triplicates and incubated for 48 h. The inserts were removed and pictures of four regions per well were taken under 4x objective of Nikon light microscope. The number of cells was calculated using ImageJ software.

For the invasion assay we used 25 μ l of matrigel which was applied to each insert in triplicates. In 48 h the inserts were twice washed with 1x PBS and fixed for 15 minutes with 4% PFA. After fixation, the cells were washed twice with 1x PBS and stained for 10 min with 10 μ g/ml Hoechst dye. Cells were again washed with 1x PBS pictures were taken.

Results

The overexpression of SK1 was a subject of numerous studies showing its association with poor overall survival of cancer patients [71,92,93]. To elucidate the importance of SK1 in lung cancer, we knock out its expression in lung adenocarcinoma cells in order to investigate its role on cell proliferation, migration and survival.

Generation of KP cells deficient in SK1 expression

To produce cells lacking SK1 (KP^{ΔSK1}) expression, we used CRISPR-Cas9 technology targeting the 2nd exon of the SK1 gene (*Sphk1*) in KRAS-mutated KP cells. In this system, Cas9 nuclease introduces a double-stranded break in the region of interest guided by specific sgRNA. The cellular DNA repair mechanism is prone to errors, hence the insertions or deletions (so-called indels) are often introduced. We have designed our sgRNA with the aim to target the 5' end of the 2nd exon so that repair mechanism with indel introduction will occur causing a frameshift; thus the expression of SK1 will be abrogated.

To confirm the indel introduction, we utilised the TIDE tool [94]. For this, we designed primers spanning possible CRISPR-Cas9-sgRNA targeting site and used them for amplification of the region of interest. The resulting sequences were subjected to TIDE analyses and predicted indels were estimated. Once the putative pool KP^{ΔSK1} was further analysed, the single clones were generated and again analysed via the TIDE tool (Fig. 8).

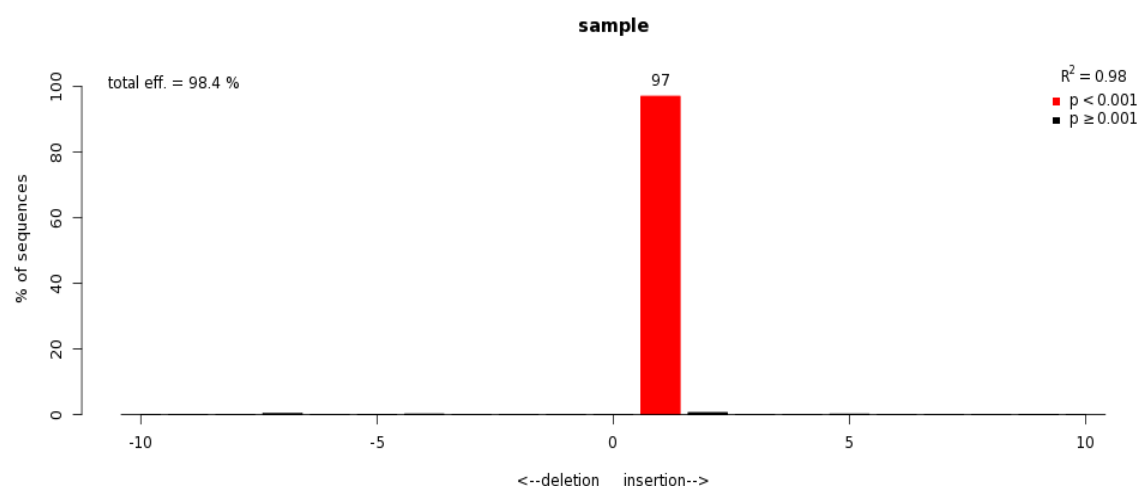


Figure 8. TIDE analysis of knock-out clone. The TIDE online platform was used to determine knock-out efficiency of SK1. The efficiency of one clone was 98.4 % with one predominant +1 indel.

One of the single $KP^{\Delta SK1}$ clones showed a single cytosine insertion which resulted in the frame-shift and premature stop codon formation (Fig. 9A). The absence of SK1 was also verified on an mRNA and a protein levels via western blotting (Fig. 9B-C).

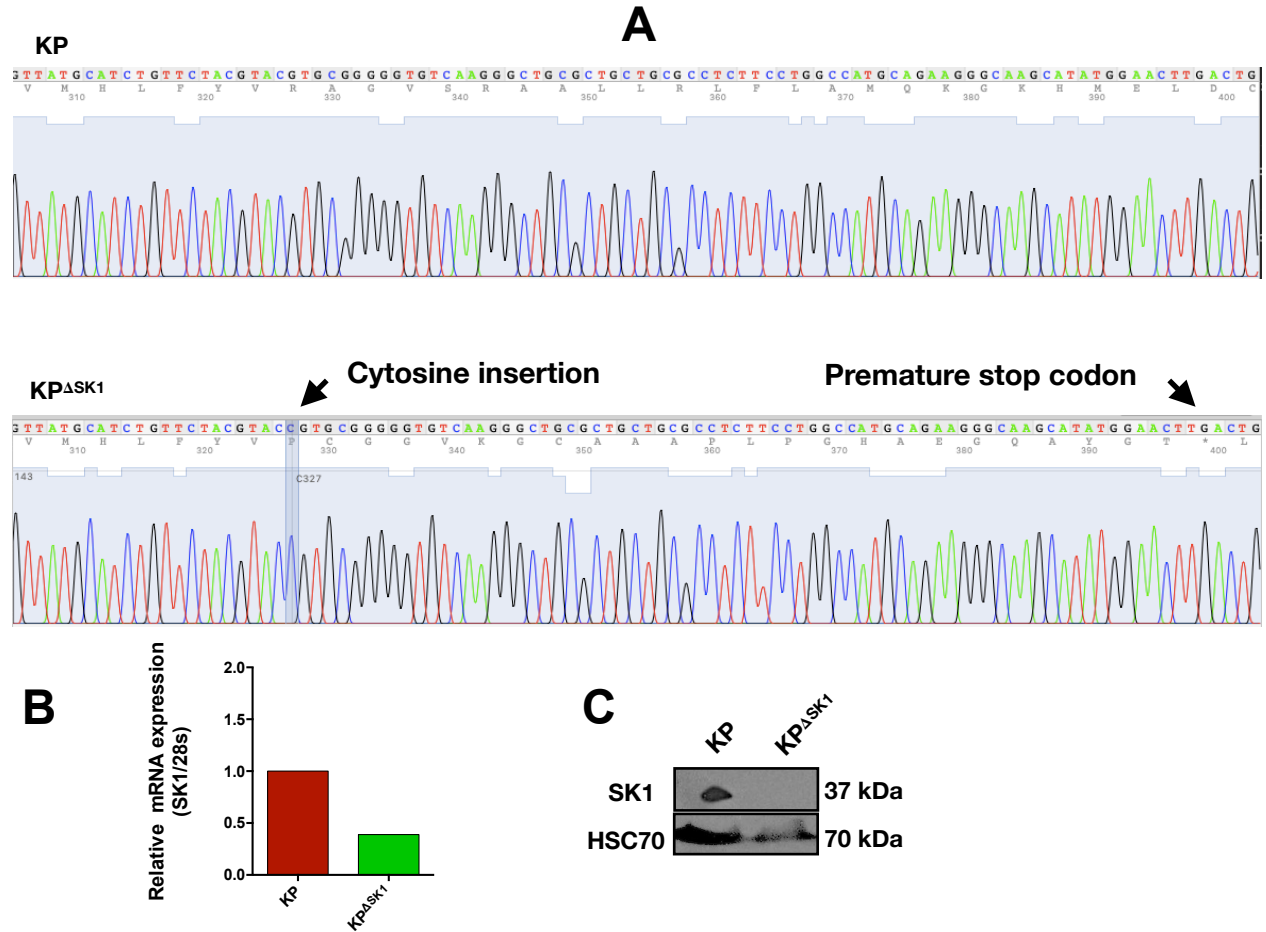


Figure 9. Verification of $KP^{\Delta SK1}$ clone. **A)** Alignment of sequences from SK1 control and $KP^{\Delta SK1}$ clone. **B)** Expression of SK1 in control and $KP^{\Delta SK1}$ cells. **C)** Western blot analyses of SK1 expression in control and $KP^{\Delta SK1}$ cells. A549, A549 Δ SK1 and EGFRdT cells were used as controls for absence and presence of SK1 expression in different cell lines.

Cells lacking SK1 exhibited changed morphology with profound movement and filopodia formation

We started our characterisation of the $KP^{\Delta SK1}$ cell phenotype by using light microscopy where we wanted to analyse the morphology of the cell. Interestingly, while the control KP cells exhibited a phenotype typical for many epithelial cell lines, such as cells were in tight contact with each other and populated any empty space, the $KP^{\Delta SK1}$ cells showed reduced cell-cell contact and were randomly distributed within the plate.

Moreover, $KP^{\Delta SK1}$ cells were forming extensive filopodia/lamellipodia-like structures which were not necessarily directed towards the neighbouring cells. Even in highly confluent conditions, when the contact between the cells was inevitable, $KP^{\Delta SK1}$ cells continued the formation of filopodia/lamellipodia-like structures (Fig. 10).

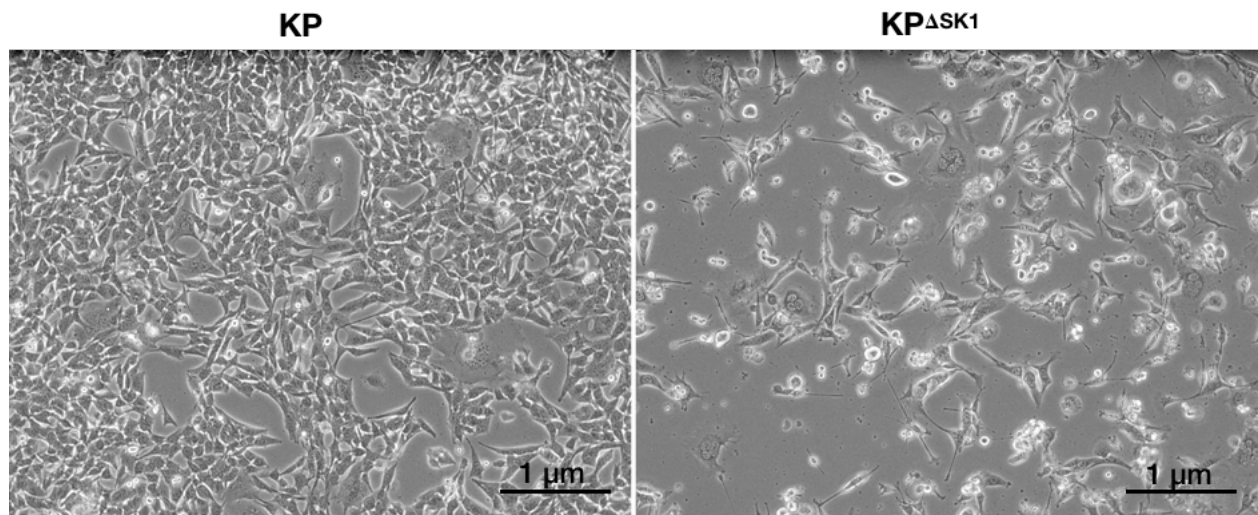


Figure 10. Morphological differences between control and $KP^{\Delta SK1}$ cells.

The time-lapse microscopy revealed an extensive movement of $KP^{\Delta SK1}$ cells compared to KP control. Although KP cells movement was eventually constrained by the neighboring cells occupying the empty space in the plate, the $KP^{\Delta SK1}$ cells continued to move regardless of the frequent contact with other cells and their filopodia/lamellipodia. To our regret, it was not possible to measure/quantify the movement of $KP^{\Delta SK1}$ cells due to their fast movement and intrinsic feature to form a bilayer of rounded cells attached on top of the moving cells (<https://data.mendeley.com/datasets/hpn8ptr5rw/1>). For this purpose, a specific artificial intelligence algorithm has to be created. Nevertheless, the time-lapse microscopy helped to visually observe the morphological difference and movement pattern due to its higher resolution and time-lapse imaging.

Cells deficient in SK1 demonstrated reduced proliferation efficiency

To test whether deficiency of SK1 can affect cell migration, wound-healing and proliferation assays were used. An inflicted gap in the wound-healing assay allows cells to migrate towards the cell-free space, thus the movement can be assessed. The pictures taken at 24 and 48 h time points revealed that KP cells were able to fully close

the wound after 48 h. In contrast, $KP^{\Delta SK1}$ cells repeatedly showed reduced capacity to completely populate the gap (Fig. 11A-C.) [91].

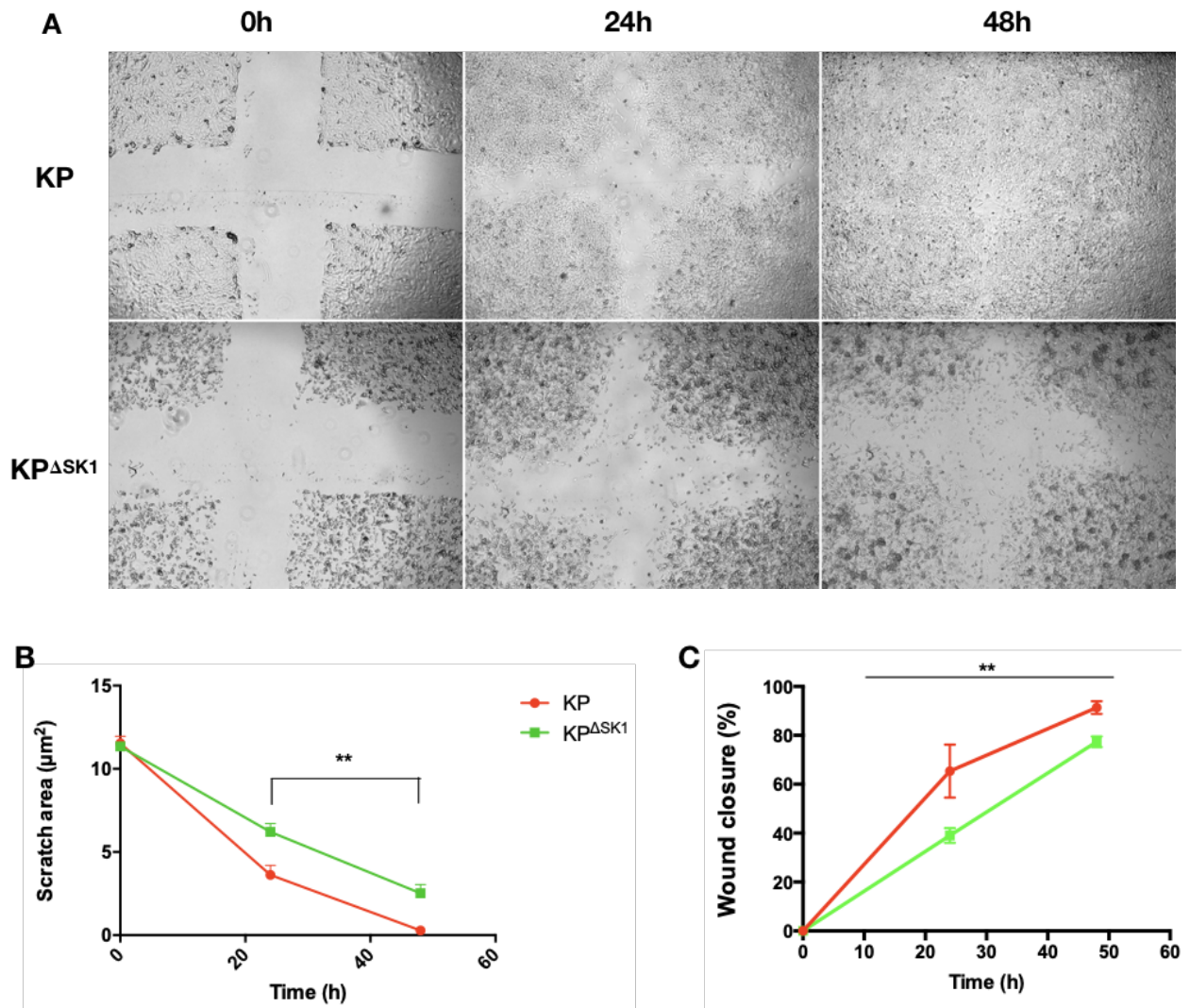


Figure 11. Wound healing assay. A) Analysis of control and $KP^{\Delta SK1}$ cells to close the wound during 48-h period. **B)** Scratch area in 48 h, $KP^{\Delta SK1}$ cells did not close the wound. **C)** Percentage of wound closure, only ~ 70% of the wound area were covered by $KP^{\Delta SK1}$. Two-way ANOVA ($\alpha < 0.05$).

The proliferation assay, where cells were harvested to be counted every 24 h for a time period of four days, a similar pattern was noticed. While the number of KP cells steadily increased with the significant jump at 96 h (almost ~ 6 times increase in proliferation), $KP^{\Delta SK1}$ cells exhibited statistically significant decrease in proliferation compared to their control counterparts (Fig. 12).

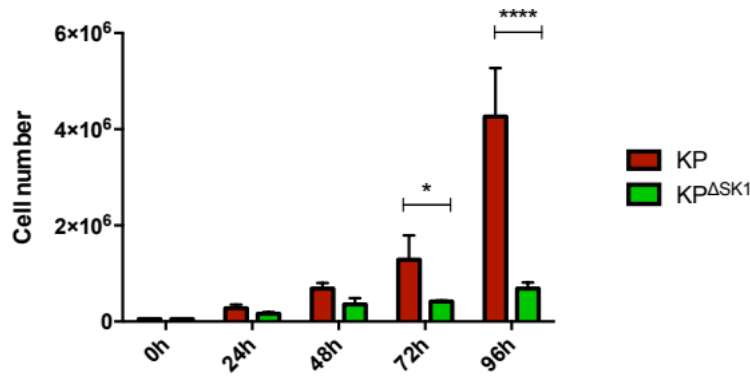


Figure 12. Comparison in proliferation pattern of KP Δ SK1 and KP control cells. At 72 h KP Δ SK1 cells continued proliferate less compared to control reaching the highest drop in proliferation capacity at 96 h. Control KP cells proliferate faster than KP Δ SK1 cells. Two-way ANOVA (alpha < 0.05).

While the proliferation capacity of KP Δ SK1 cells was reduced in the wound-healing assay, the notable diminished proliferation might be due to the everyday trypsinization of cells and/or the inability of KP Δ SK1 cells to quickly produce vital proteins for cell attachment, movement, and subsequent division.

KP Δ SK1 cells showed random cell motility and lack of monolayer formation

To assess whether KP Δ SK1 cells display possible directionally in their movement, we decided to use fluorescent microscopy. For this, we created GFP-expressing KP and KP Δ SK1 cells (further KP_GFP and KP Δ SK1_GFP) using GFP-expressing lentivirus. The control non-fluorescent cells and cells expressing GFP were plated in 12 well-plate (1:1) so that the difference in cell movement can be observed at 24h of co-culturing. As seen in Figure 13, KP cells migrate in closely associated groups forming a monolayer. In contrast, KP Δ SK1 cells exhibit random single-cell movement and lack of monolayer formation. Interestingly, we have noticed a slight change in KP Δ SK1 cells abundance when co-cultured with KP cells (KP-KP Δ SK1 image). This led us to suspect that KP cells release compound which can affect KP Δ SK1 cells proliferation.

24h

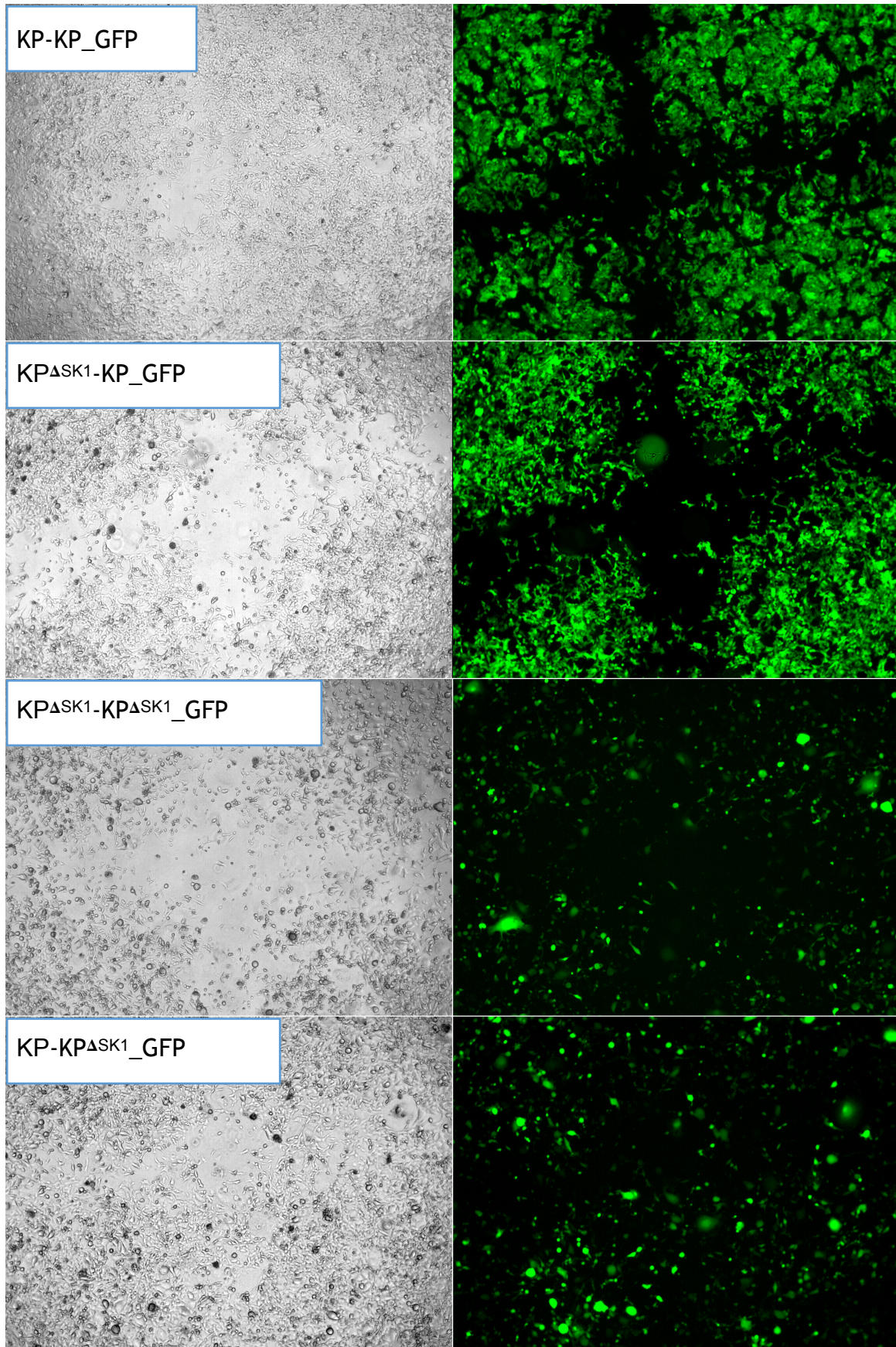


Figure 13. Fluorescent migration assay 24 h after wound introduction. Control (KP) cells form cellular sheets while KP Δ SK1 cells do not exhibit tight associations between the cells and freely move around whole area.

Sphingosine-1-phosphate is not able to rescue the proliferation capacity of $KP^{\Delta SK1}$ cells

To check the ability of sphingosine-1-phosphate (S1P) to influence $KP^{\Delta SK1}$ proliferation, we performed FACS analysis of co-cultured $KP^{\Delta SK1}$ and KP cells. For this, we used specific CellTrace™ dyes (violet and CFSE) allowing us to distinguish and track multiple cellular generations along with discrimination between our single- or co-cultures at a time point of 72 h. These dyes are cell-permeable non-fluorescent esters of amine-reactive fluorescent molecules which upon cell entrance are converted to a fluorescent derivative by cellular esterases, leading to proteins' amine groups binding and consequently long-term cellular retention. Upon division, each daughter cell receives approximately half of the fluorescent label from their parental cell, thus enabling tracking cells for multiple generations.

To clearly distinguish every generation, we stained cells with the mentioned dyes every other day upon harvesting for FACS analysis. We also included two additional controls when $KP^{\Delta SK1}$ cells were stained independently with both of each dyes and then mixed together. Same experimental protocol was used for KP cells. These controls were performed in order to test the possible dye effects on cell viability. In addition, we included a live-dead marker (yellow) to clearly distinguish the dead-cell population. The analysis of three independent experiments demonstrated that S1P or other secreted factors released from KP cells with did not recover the proliferation capacity of $KP^{\Delta SK1}$ cells (Fig. 14).

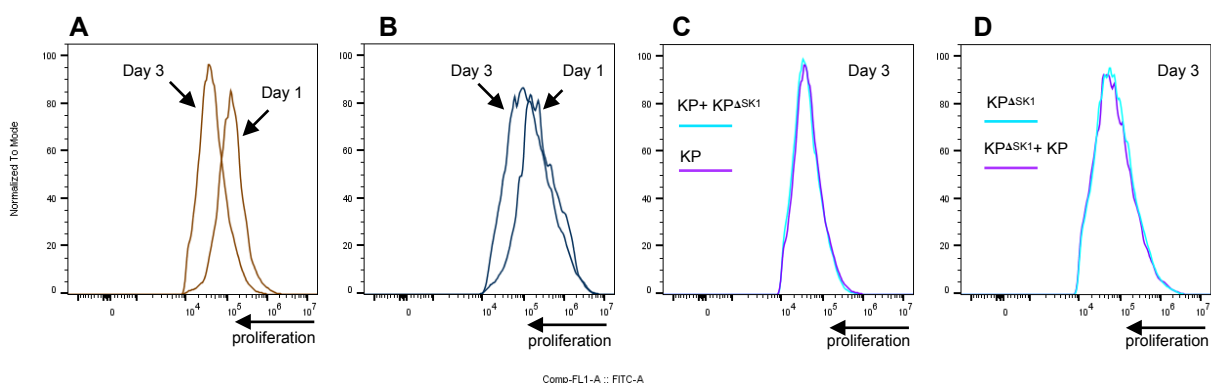


Figure 14. FACS analysis. Coculturing of $KP^{\Delta SK1}$ with control KP cells did not result in increased proliferation capacity. **A)** Proliferation of KP cells at 24 h and 72 h. **B)** Proliferation of $KP^{\Delta SK1}$ cells at 24 h and 72 h. **C)** Proliferation of KP cells (violet) compared with KP cocultured with $KP^{\Delta SK1}$ cells (magenta) at 72 h. **D)** Comparison of proliferation of $KP^{\Delta SK1}$ cells (blue) with $KP^{\Delta SK1}$ cocultured with KP cells (magenta) at 72 h.

To reconfirm these results, we have decided to perform a rescue experiment for $KP^{\Delta SK1}$ cells by using the supernatant of KP cells and vice versa. It is known that S1P acts in an autocrine and paracrine manner and its release from the cells could affect $KP^{\Delta SK1}$ cells. Thus, we plated 5×10^5 cells of each cell line and collected supernatants after 24 h. Next, the same cell number was plated into 6 cm Petri dishes, and the supernatant from KP cells was applied to $KP^{\Delta SK1}$ cells, while the supernatant from $KP^{\Delta SK1}$ cells was added to KP cells. For both, the complete media was added in a 1:1 ratio to the supernatants to supply cells with vital amino acids and with the final FBS concentration to 10% to mimic the normal environment. As additional controls, both KP and $KP^{\Delta SK1}$ cells were substituted with their own supernatants. After 48 h, we harvested and counted the cells. Our results from the rescue experiment verified that the supernatant of KP cells, which should contain S1P, failed to rescue the proliferation capacity of $KP^{\Delta SK1}$ cells (Fig. 15).

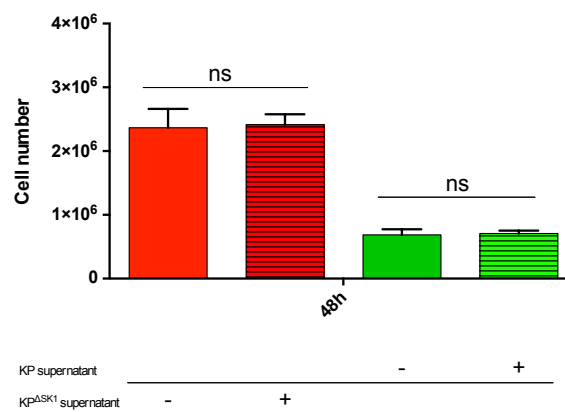


Figure 15. Rescue capacity of S1P. S1P or other secreted factors contained in the supernatant of control KP cells were not affecting proliferation capacity of $KP^{\Delta SK1}$ cells.

$KP^{\Delta SK1}$ cells exhibited increased movement but reduced invasiveness compared to KP cells

To confirm whether the migration pattern of $KP^{\Delta SK1}$ and KP cells from the 2D settings translates into the 3D environment, we performed the transwell assay. This assay tests the ability of cells for chemotaxis. For this, we used specific transwell inserts containing membranes with 8 μ m pores. The 10% concentration of serum in the medium in the 12 well-plates and the 2% in the inserts served as a chemoattractant for the plated cells. After 48 h incubation, we observed the significant movement of $KP^{\Delta SK1}$ cells

into the lower chamber compared to KP cells. This result shows increased movement of $KP^{\Delta SK1}$ cells in 3D culture which was previously observed for our 2D co-culture experiments. However, the extensive movement does not indicate invasion ability of these cells (Fig. 16).

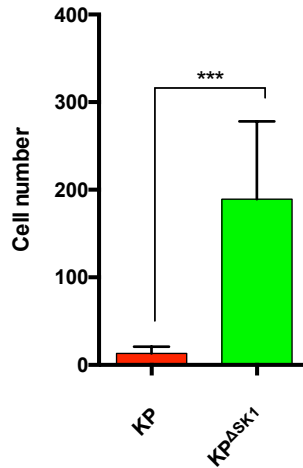


Figure 16. Transwell assay. $KP^{\Delta SK1}$ cells exhibit profound migration toward chemoattractant compared to control KP cells. Two-way ANOVA ($\alpha < 0.05$).

To study the invasion capacity of the $KP^{\Delta SK1}$ cell, we performed the same assay with addition of matrigel as a tool to mimic an extracellular environment/matrix [93]. After 48 h analysis demonstrated that $KP^{\Delta SK1}$ cell were able to degrade matrix proteins showing invasion ability. However, to our surprise KP cells showed significantly greater invasiveness compared to $KP^{\Delta SK1}$ cells (Fig. 17). Comparison of both migration and invasion transwell assays led us to suspect that lack of SK1 promotes cell migration but reduces the invasion capacity of KO cells.

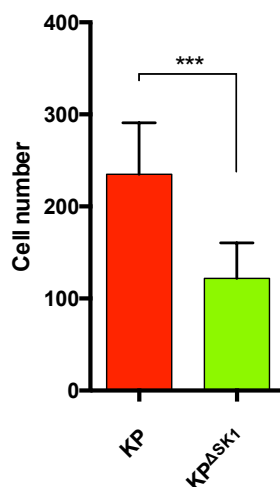


Figure 17. Transwell invasion assay. $KP^{\Delta SK1}$ cells exhibit less invasiveness compared to control KP cells. Two-way ANOVA ($\alpha < 0.05$).

KP^{ΔSK1} cells revealed specific expression profile

To further dissect the KP^{ΔSK1} morphological features, we aimed to investigate the transcriptional profile of these cells including possible alterations in the expression of immune checkpoint molecules compared to control cells. Specifically, we were interested in genes responsible for the cell-cell junctions, adhesion, and movement as they were shown to greatly facilitate metastatic potential of cancer cells as well as PD-L1 and other genes implicated in cancer. For this, we performed an RT-qPCR analysis of KP and KP^{ΔSK1} cells with three technical and biological replicates.

The two genes coding for E-Cadherin (*CDH1*) and N-Cadherin (*CDH2*) were downregulated while the gene for the β -Catenin was in turn slightly upregulated in KP^{ΔSK1} cells. Interestingly, all three proteins play important roles in the cell-cell junctions, cellular adhesions, epithelial to mesenchymal transitions, and were shown to be implicated in cancer. In addition, β -Catenin has a second function in Wnt signalling which is involved in autocrine/paracrine cell communications and its misregulation leads to cancer development. The expression of *Snai1/2* genes, which are involved in the regulation of adhesion molecules, and *VIM*, a member of intermediate filaments protein family, were not affected in KP^{ΔSK1} cells (Fig. 17A).

We were also interested in Fascin1 protein. Fascin 1 is an actin-bundling protein that was shown to be involved in metastasis upon its overexpression. Here, we observed almost complete abrogation of mRNA production in KP^{ΔSK1} cells which was further supported on the protein level by western blotting (Fig. 17B). *HIF1A* gene is known for its response to cellular and developmental hypoxia. Its misregulation was shown in many cancer types with aggressive tumor progression. In our KP^{ΔSK1} cell, the relative expression of this gene was almost twice higher than in control KP cells (Fig. 17C). With regard to the PD-L1 expression, we did not notice any difference in the gene expression profile between both cell lines.

Overall, these alterations in gene expression profiles might explain the phenotypic features of KP^{ΔSK1} cells. For instance, the low potential to form cell-cell junctions' can result in increased random movement and lack of monolayer formation or significantly lower proliferation capacity compared to control KP cells.

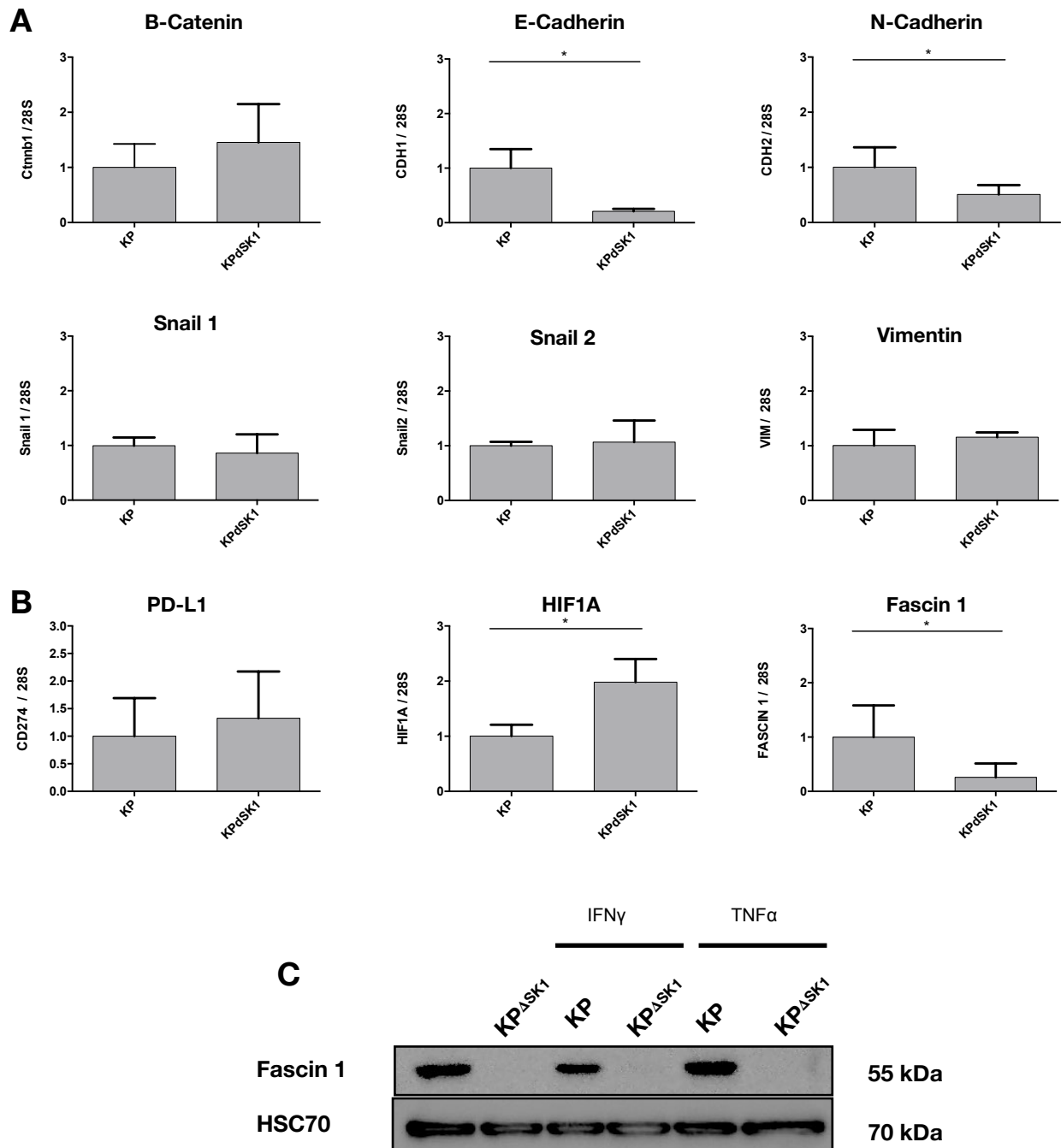


Figure 17. Relative mRNA expression. A) *CDH1* and *CDH2* genes are downregulated in KP Δ SK1 cells. **B)** *HIF1A* is overexpressed while *Fascin1* significantly downregulated in KP Δ SK1 cells. **C)** Downregulation of Fascin1 expression is confirmed on a protein level. Student T-test ($p < 0.05$)

Discussion

Genetic alterations in oncogenes along with the tumor suppressors frequently lead to tumorigenesis. In lung cancer, the most common mutations happen in KRAS, EGFR, and p53 genes. The KRAS-associated tumors frequently emerge from epithelial

cells subjected to persistent pro-inflammatory signals and constant environmental stress (e.g. smoking) while EGFRs are common in non-smokers. KRAS mutants induce expression of pro-inflammatory NF- κ B and cooperate with Myc, known for its immunosuppression function [97,98]. PD-L1, the immune checkpoint like programmed death-ligand 1 which prevents T cells from killing cancer cells, is highly expressed in KRAS LUAC [99]. Moreover, the potent anti-inflammatory A20 protein was recently shown to be downregulated helping cancer cells evade tight immune control, thus tuning the tumor microenvironment[100]. While EGFR tumors more often respond to current antitumor therapies, KRAS-associated tumors are notoriously difficult to treat.

The intrinsic feature of any cancer cells is their ability to rapid proliferation and constant alterations in signalling profiles to escape host immunological response. Due to the genetic heterogeneity of lung cancers, tumor cells are prone to quick resistance development if subjected to monotherapy. At present, combined therapies proved to be a game-changer in lung cancer treatment, thus the search for new target molecules is of utmost importance. The overexpression of SK1 was shown to play an important role in breast, colon, prostate, and lung cancer progression [70–72]. This makes SK1 a promising target and could probably show clinical benefits if combined with other cancer therapies. Intriguingly, our laboratory performed a high-throughput afatinib-based screening (tyrosine kinase inhibitor used for NSCLC treatment) to identify any potential molecules able to boost the efficacy of afatinib in KRAS-associated tumors and SK1 was shown to be a promising target. Hence, the main goal of this study was to unravel the role of the SK1 in the growth, survival, and potential oncogenic signalling pathways of tumor cells.

Morphologic description of KP cancer cells lacking SK1

To characterize the role of SK1 in lung adenocarcinomas (murine KP cells), we took advantage of widely used CRISPR/Cas9 technology. It enabled us to create a cell line with a complete deficiency of SK1 expression rather than just silencing it with a chance of leakage and subsequent alterations in the results. The absence of SK1 expression we confirmed both on mRNA and protein expression levels.

Interestingly, the absence of SK1 led to a significantly altered morphology of KP ^{Δ SK1} cells compared to the parental cell line. In particular, we observed the extended filopodia formation typical for characteristics of mesenchymal cells [101]. It was shown that the transition between epithelial to mesenchymal phenotype is associated with the

cytoskeleton remodeling. These cellular filopodia/lamellipodia-like structures of KP Δ SK1 are not temporary features that are common for trypsinized cells to adhere to the surfaces and create cell-to-cell contacts but are an intrinsic feature of KP Δ SK1 cells. Moreover, even in a densely populated environment, KP Δ SK1 cells still exhibit prominent filopodia development. However, this specific KP Δ SK1 feature is not applicable for example to the breast cancer study where cells lacking SK1 expression exhibited rounded morphology compared to control cells [96]. The mentioned study used shRNA to abrogate SK1 expression, which could potentially lead to a small SK1 leakage and other mechanisms responsible for the changed morphology.

Nevertheless, the potential mesenchymal phenotype of our KP Δ SK1 cells is supported by analysis of gene profiles molecules that are responsible for cell-cell adhesion, interactions, and communications. For instance, adhesion proteins like cadherins are located on the cell membranes of adjacent cells and thus sealing the adjacent cells to each other and helping in tissue formation. The downregulation of both E-cadherin and N-cadherin can abrogate vital cellular connections leading to the observed mesenchymal phenotype. On the other hand, we noticed elevated β -Catenin expression. β -Catenin connects cadherins to cytoskeletal proteins and is involved in Wnt signalling. Wnt is a known signalling pathway activated during epithelial-to-mesenchymal transition thus it well supports the mesenchymal morphology of KP Δ SK1 cells. Altogether, these results indicate a considerable role of SK1 is in the maintenance of the cellular structure and organisation.

SK1 ablation leads to reduced proliferation, invasiveness and increased motility

Since the intrinsic feature of cancer cells is characterised by their rapid proliferation and survival, we speculated that knock-out of SK1 would result in a decreased ability of KP cells to proliferate via ablation of S1P signalling. To determine the proliferative capacity of KP Δ SK1 cells, we performed two experiments: the wound-healing assay and the proliferation assay. The wound-healing assay also provides an insight into the migration pattern of cells.

The wound-healing assays showed inability of KP Δ SK1 cells to completely close the wound in comparison to the parental KP cells. During the proliferation assay, when cells were harvested each 24 h for three days, we observed a reduction in proliferation

as well. However, this reduction was more statistically striking than in the wound-healing assay. One might argue that everyday trypsinization might affect the proliferation capacity of KP Δ SK1 cells which we well support. Nevertheless, while maintaining KP and KP Δ SK1 cells we observed results similar to wound-healing assay (data not shown here).

The collective migration is an indispensable hallmark of cancer cells to promote invasion and metastasis [102]. To assess the cellular migration of KP Δ SK1 cells we created GFP expressing KP Δ SK1 and KP cells to be able to co-culture them and discriminate between the KO and parental cell line. In addition, we wanted to investigate whether KP can affect KP Δ SK1 cells if co-cultured. For this, we generated GFP-expressing lentiviruses and transduced both KP and KP Δ SK1 cells. Unfortunately, we were not able to produce RFP-expressing cell lines for better representation due to the problem with the RFP expression vector. So we again performed a wound-healing assay but added two additional conditions where KP Δ SK1_GFP cells were co-cultured with KP lacking GFP and vice versa. Our results showed that the KP Δ SK1_GFP cells were not able to re-populate the inflicted wound. In addition, we observed the random movement of these cells. Compared to KP_GFP, which were moving in closely-associated groups forming cell sheets, KP Δ SK1_GFP cells were randomly distributed and did not form closely-associated groups. Since we had KP cells expressing dTomato (although not the parental KP but genetically similar) we decided to perform an additional wound-healing experiment to better visualise the difference between KPdTomo and KP Δ SK1_GFP cells. As expected, KPdTomo cells followed the same pattern of movement and sheet formation while KP Δ SK1_GFP cells were randomly distributed (Fig. S1).

Based on these results, we conclude that the SK1 might be responsible for cellular proliferation with the implication to form closely associated groups vital for the efficient spread and survival of cancer cells. Although one may argue that increased cell motility may result in faster metastatic potential, the misregulation of the adhesive molecules may prevent better invasiveness of these cells as noticed in the 104T melanoma cell line [103]. It is worth mentioning that cell motility is not equal to cell spreading due to their mechanistically different patterns [104]. Indeed, the results from both migration and invasion transwell assays supported this notion. Although migratory pattern of KP Δ SK1 cells was significantly higher compared to parental cells, the invasion capacity was notably lower than in the case of KP cells.

S1P is not able to rescue $KP^{\Delta SK1}$ cellular phenotype

Due to the tight axis between S1P and SK1, and the broad implications of S1P signalling, we were wondering whether S1P could rescue the proliferative capacity of the $KP^{\Delta SK1}$ cells. At first, we took advantage of specific proliferation dyes for FACS analysis where cells were stained with different dyes, mixed together, and analysed after 72h. These three independent experiments demonstrated inability of KP cells to increase proliferation capacity of $KP^{\Delta SK1}$ cells.

Next, we performed an additional experiment to support our FACS results. Therefore, we collected the supernatant from both KP and $KP^{\Delta SK1}$ cells. The KP supernatant with or without supplements described in the results and method sections was added to freshly plated $KP^{\Delta SK1}$ cells while $KP^{\Delta SK1}$ supernatant was added to KP cells in the same manner. Regardless of additives, we observed no difference in proliferative capacities of both cell lines meaning that S1P is not able to influence or rescue the phenotype of $KP^{\Delta SK1}$ cells. Indeed, the proper cellular adhesion is thought to be a prerequisite for the correct functioning of cellular receptors [105]. Via improper expression of adhesion and cell-junction proteins, the SK1 abrogation might indirectly lead to improper functioning of S1P receptors which can explain why the supernatant of KP cells containing S1P was not able to rescue the phenotype of $KP^{\Delta SK1}$ cells. However, it might be possible that $KP^{\Delta SK1}$ biology might be receptor independent which could potentially in anyways be an advantage for cancer treatment.

Conclusion and outlook of this study

In this study, we showed that deletion of SK1 caused significant drop in proliferation capacity of KRAS-mutated mouse adenocarcinoma cells. Moreover, the accompanying morphological changes resulted in extensive filopodia/lamellapodia formation, increased random movements but decreased invasiveness which is in line with the study on metastatic potential of SK1 in triple-breast cancer [96]. Here we demonstrated that expression of Fascin 1, the protein involved in metastasis, was abrogated in $KP^{\Delta SK1}$ cells. In addition, we assessed the mesenchymal gene expression profile which is important for cancer cells to acquire a mobility pattern for migration from the primary sites. In our $KP^{\Delta SK1}$ cells, E-cadherin and N-cadherin expressing genes vital for epithelial-mesenchymal transition [106] were downregulated. The underlying mechanism of increased migration pattern of $KP^{\Delta SK1}$ cells is yet to be elucidated. Finally,

we showed that the biological SK1 is rather intracellular and cannot be rescued by its product, S1P.

In conclusion, this study was focused on elucidation of the biological role of SK1 *in vitro* KRAS-mutated murine adenocarcinoma model. It is needed to test these results on *in vivo* models as it might produce a different outlook. For example, to test the metastatic potential of $KP^{\Delta SK1}$ cells we can use $KP^{\Delta SK1}$ -GFP cells transplanted to mice. The FACS analysis of cells from lungs, spleen and kidneys could potentially show the distribution of fluorescently labelled cells. Lastly, the KRAS-driven adenocarcinoma was shown to respond to a pan-ErbB inhibitor, afatinib [107]. However, the application of afatinib as a monotherapy could lead to tumor resistance. Hence, the potentially advantageous synergism of SK1 targeting along with simultaneous application of afatinib can be tested in KRAS-mutated model *in vivo* .

References

1. Lung Cancer in Austria. *J Thorac Oncol.* 2021;16: 725–733.
2. Jemal A, Bray F, Melissa M. Center, Ferlay J, Ward E, Forman D. Global cancer statistics. *CA: A Cancer Journal for Clinicians.* 2011. pp. 69–90. doi:10.3322/caac.20107
3. Planchard D, Popat S, Kerr K, Novello S, Smit EF, Faivre-Finn C, et al. Metastatic non-small cell lung cancer: ESMO Clinical Practice Guidelines for diagnosis, treatment and follow-up. *Ann Oncol.* 2018;29: iv192–iv237.
4. Sutherland KD, Proost N, Brouns I, Adriaensen D, Song J-Y, Berns A. Cell of origin of small cell lung cancer: inactivation of Trp53 and Rb1 in distinct cell types of adult mouse lung. *Cancer Cell.* 2011;19: 754–764.
5. Cagle PT, Allen TC, Olsen RJ. Lung cancer biomarkers: present status and future developments. *Arch Pathol Lab Med.* 2013;137: 1191–1198.
6. Burghuber OC, Kirchbacher K, Mohn-Staudner A, Hochmair M, Breyer M-K, Studnicka M, et al. Results of the Austrian National Lung Cancer Audit. *Clin Med Insights Oncol.* 2020;14: 1179554920950548.
7. Risch A, Plass C. Lung cancer epigenetics and genetics. *Int J Cancer.* 2008;123: 1–7.
8. Larsen JE, Minna JD. Molecular biology of lung cancer: clinical implications. *Clin Chest Med.* 2011;32: 703–740.
9. Zito Marino F, Bianco R, Accardo M, Ronchi A, Cozzolino I, Morgillo F, et al. Molecular heterogeneity in lung cancer: from mechanisms of origin to clinical implications. *Int J Med Sci.* 2019;16: 981–989.
10. Wistuba II, Gazdar AF. Lung cancer preneoplasia. *Annu Rev Pathol.* 2006;1: 331–348.
11. Kohno T, Nakaoku T, Tsuta K, Tsuchihara K, Matsumoto S, Yoh K, et al. Beyond ALK-RET, ROS1 and other oncogene fusions in lung cancer. *Transl Lung Cancer Res.* 2015;4: 156–164.
12. Johnson L, Greenbaum D, Cichowski K, Mercer K, Murphy E, Schmitt E, et al. K-ras is an essential gene in the mouse with partial functional overlap with N-ras. *Genes Dev.* 1997;11: 2468–2481.
13. Karnoub AE, Weinberg RA. Ras oncogenes: split personalities. *Nat Rev Mol Cell Biol.* 2008;9: 517–531.
14. Campbell SL, Khosravi-Far R, Rossman KL, Clark GJ, Der CJ. Increasing complexity of Ras signaling. *Oncogene.* 1998;17: 1395–1413.
15. Downward J. Targeting RAS signalling pathways in cancer therapy. *Nat Rev Cancer.* 2003;3: 11–22.
16. Cooper WA, Lam DCL, O’Toole SA, Minna JD. Molecular biology of lung cancer. *J Thorac Dis.* 2013;5 Suppl 5: S479–90.
17. Hobbs GA, Aaron Hobbs G, Der CJ, Rossman KL. RAS isoforms and mutations in cancer at a glance. *Journal of Cell Science.* 2016. doi:10.1242/jcs.182873
18. Moore AR, Rosenberg SC, McCormick F, Malek S. Author Correction: RAS-targeted therapies: is the undruggable drugged? *Nat Rev Drug Discov.* 2020;19: 902.

19. Molina-Arcas M, Samani A, Downward J. Drugging the Undruggable: Advances on RAS Targeting in Cancer. *Genes* . 2021;12. doi:10.3390/genes12060899
20. Kitajima S, Thummalapalli R, Barbie DA. Inflammation as a driver and vulnerability of KRAS mediated oncogenesis. *Semin Cell Dev Biol*. 2016;58: 127–135.
21. Fujimura T, Kambayashi Y, Ohuchi K, Muto Y, Aiba S. Treatment of Advanced Melanoma: Past, Present and Future. *Life*. 2020;10. doi:10.3390/life10090208
22. Canon J, Rex K, Saiki AY, Mohr C, Cooke K, Bagal D, et al. The clinical KRAS(G12C) inhibitor AMG 510 drives anti-tumour immunity. *Nature*. 2019;575: 217–223.
23. Hallin J, Engstrom LD, Hargis L, Calinisan A, Aranda R, Briere DM, et al. The KRAS Inhibitor MRTX849 Provides Insight toward Therapeutic Susceptibility of KRAS-Mutant Cancers in Mouse Models and Patients. *Cancer Discov*. 2020;10: 54–71.
24. Nakajima H, Kotani D, Bando H, Kato T, Oki E, Shinozaki E, et al. REMARRY and PURSUIT trials: liquid biopsy-guided rechallenge with anti-epidermal growth factor receptor (EGFR) therapy with panitumumab plus irinotecan for patients with plasma RAS wild-type metastatic colorectal cancer. *BMC Cancer*. 2021;21: 674.
25. Scheffler M, Ihle MA, Hein R, Merkelbach-Bruse S, Scheel AH, Siemanowski J, et al. K-ras Mutation Subtypes in NSCLC and Associated Co-occurring Mutations in Other Oncogenic Pathways. *J Thorac Oncol*. 2019;14: 606–616.
26. Scagliotti GV, Selvaggi G, Novello S, Hirsch FR. The biology of epidermal growth factor receptor in lung cancer. *Clin Cancer Res*. 2004;10: 4227s–4232s.
27. Lynch TJ, Bell DW, Sordella R, Gurubhagavatula S, Okimoto RA, Brannigan BW, et al. Activating mutations in the epidermal growth factor receptor underlying responsiveness of non-small-cell lung cancer to gefitinib. *N Engl J Med*. 2004;350: 2129–2139.
28. Paez JG, Jänne PA, Lee JC, Tracy S, Greulich H, Gabriel S, et al. EGFR mutations in lung cancer: correlation with clinical response to gefitinib therapy. *Science*. 2004;304: 1497–1500.
29. da Cunha Santos G, Shepherd FA, Tsao MS. EGFR mutations and lung cancer. *Annu Rev Pathol*. 2011;6: 49–69.
30. Choong NW, Dietrich S, Seiwert TY, Tretiakova MS, Nallasura V, Davies GC, et al. Gefitinib response of erlotinib-refractory lung cancer involving meninges--role of EGFR mutation. *Nat Clin Pract Oncol*. 2006;3: 50–7; quiz 1 p following 57.
31. Castellanos E, Feld E, Horn L. Driven by Mutations: The Predictive Value of Mutation Subtype in EGFR-Mutated Non-Small Cell Lung Cancer. *J Thorac Oncol*. 2017;12: 612–623.
32. Harvey RD, Adams VR, Beardslee T, Medina P. Afatinib for the treatment of EGFR mutation-positive NSCLC: A review of clinical findings. *J Oncol Pharm Pract*. 2020;26: 1461–1474.
33. Soria J-C, Ohe Y, Vansteenkiste J, Reungwetwattana T, Chewaskulyong B, Lee KH, et al. Osimertinib in Untreated EGFR-mutated advanced non-small-cell lung cancer. *N Engl J Med*. 2018;378: 113–125.
34. Leonetti A, Sharma S, Minari R, Perego P, Giovannetti E, Tiseo M. Resistance mechanisms to osimertinib in EGFR-mutated non-small cell lung cancer. *Br J Cancer*. 2019;121: 725–737.
35. Hanahan D, Weinberg RA. Hallmarks of cancer: the next generation. *Cell*. 2011;144: 646–674.

36. Köhler J, Jänne PA. If Virchow and Ehrlich Had Dreamt Together: What the Future Holds for Mutant Lung Cancer. *Int J Mol Sci.* 2021;22. doi:10.3390/ijms22063025
37. Dunn GP, Old LJ, Schreiber RD. The three Es of cancer immunoediting. *Annu Rev Immunol.* 2004;22: 329–360.
38. Santaniello A, Napolitano F, Servetto A, De Placido P, Silvestris N, Bianco C, et al. Tumour Microenvironment and Immune Evasion in EGFR Addicted NSCLC: Hurdles and Possibilities. *Cancers .* 2019;11. doi:10.3390/cancers11101419
39. David EA, Clark JM, Cooke DT, Melnikow J, Kelly K, Canter RJ. The Role of Thoracic Surgery in the Therapeutic Management of Metastatic Non-Small Cell Lung Cancer. *J Thorac Oncol.* 2017;12: 1636–1645.
40. Hellmann MD, Li BT, Chaft JE, Kris MG. Chemotherapy remains an essential element of personalized care for persons with lung cancers. *Ann Oncol.* 2016;27: 1829–1835.
41. Herter-Sprue GS, Koyama S, Korideck H, Hai J, Deng J, Li YY, et al. Synergy of radiotherapy and PD-1 blockade in Kras-mutant lung cancer. *JCI Insight.* 2016;1: e87415.
42. Hirsch FR, Suda K, Wiens J, Bunn PA Jr. New and emerging targeted treatments in advanced non-small-cell lung cancer. *Lancet.* 2016;388: 1012–1024.
43. Huang W, Chen J-J, Xing R, Zeng Y-C. Combination therapy: Future directions of immunotherapy in small cell lung cancer. *Transl Oncol.* 2021;14: 100889.
44. Pardoll DM. The blockade of immune checkpoints in cancer immunotherapy. *Nat Rev Cancer.* 2012;12: 252–264.
45. Onoi K, Chihara Y, Uchino J, Shimamoto T, Morimoto Y, Iwasaku M, et al. Immune Checkpoint Inhibitors for Lung Cancer Treatment: A Review. *J Clin Med Res.* 2020;9. doi: 10.3390/jcm9051362
46. Borghaei H, Paz-Ares L, Horn L, Spigel DR, Steins M, Ready NE, et al. Nivolumab versus Docetaxel in Advanced Nonsquamous Non-Small-Cell Lung Cancer. *N Engl J Med.* 2015;373: 1627–1639.
47. Rittmeyer A, Barlesi F, Waterkamp D, Park K, Ciardiello F, von Pawel J, et al. Atezolizumab versus docetaxel in patients with previously treated non-small-cell lung cancer (OAK): a phase 3, open-label, multicentre randomised controlled trial. *Lancet.* 2017;389: 255–265.
48. Herbst RS, Baas P, Kim D-W, Felip E, Pérez-Gracia JL, Han J-Y, et al. Pembrolizumab versus docetaxel for previously treated, PD-L1-positive, advanced non-small-cell lung cancer: a randomised controlled trial. *Lancet.* 2016;387: 1540–1550.
49. Dias Carvalho P, Machado AL, Martins F, Seruca R, Velho S. Targeting the Tumor Microenvironment: An Unexplored Strategy for Mutant KRAS Tumors. *Cancers .* 2019;11. doi:10.3390/cancers11122010
50. Pereira F, Ferreira A, Reis CA, Sousa MJ, Oliveira MJ, Preto A. KRAS as a Modulator of the Inflammatory Tumor Microenvironment: Therapeutic Implications. *Cells.* 2022;11. doi: 10.3390/cells11030398
51. Wolchok JD, Kluger H, Callahan MK, Postow MA, Rizvi NA, Lesokhin AM, et al. Nivolumab plus ipilimumab in advanced melanoma. *N Engl J Med.* 2013;369: 122–133.
52. Michaud M, Martins I, Sukkurwala AQ, Adjemian S, Ma Y, Pellegatti P, et al. Autophagy-dependent anticancer immune responses induced by chemotherapeutic agents in mice. *Science.* 2011;334: 1573–1577.
53. Gasser S, Orsulic S, Brown EJ, Raulet DH. The DNA damage pathway regulates innate immune system ligands of the NKG2D receptor. *Nature.* 2005;436: 1186–1190.

54. Pfannenstiel LW, McNeilly C, Xiang C, Kang K, Diaz-Montero CM, Yu JS, et al. Combination PD-1 blockade and irradiation of brain metastasis induces an effective abscopal effect in melanoma. *Oncoimmunology*. 2019;8: e1507669.
55. Ogretmen B, Hannun YA. Biologically active sphingolipids in cancer pathogenesis and treatment. *Nat Rev Cancer*. 2004;4: 604–616.
56. Shida D, Takabe K, Kapitonov D, Milstien S, Spiegel S. Targeting SphK1 as a new strategy against cancer. *Curr Drug Targets*. 2008;9: 662–673.
57. Hannun YA, Obeid LM. Sphingolipids and their metabolism in physiology and disease. *Nat Rev Mol Cell Biol*. 2018;19: 175–191.
58. Bhattacharya J. *Cell Signaling in Vascular Inflammation*. Springer Science & Business Media; 2007.
59. Maceyka M, Payne SG, Milstien S, Spiegel S. Sphingosine kinase, sphingosine-1-phosphate, and apoptosis. *Biochim Biophys Acta*. 2002;1585: 193–201.
60. Bonica J, Mao C, Obeid LM, Hannun YA. Transcriptional Regulation of Sphingosine Kinase 1. *Cells*. 2020;9. doi:10.3390/cells9112437
61. Jarman KE. *Regulation of Sphingosine Kinase 1 Signalling by Calcium- and Integrin-binding Proteins*. 2010.
62. Leclercq T, Pitson S. Cellular signalling by sphingosine kinase and sphingosine 1-phosphate. *IUBMB Life (International Union of Biochemistry and Molecular Biology: Life)*. 2006. pp. 467–472. doi:10.1080/15216540600871126
63. Alvarez SE, Milstien S, Spiegel S. Autocrine and paracrine roles of sphingosine-1-phosphate. *Trends Endocrinol Metab*. 2007;18: 300–307.
64. Spiegel S, Milstien S. Sphingosine-1-phosphate: an enigmatic signalling lipid. *Nat Rev Mol Cell Biol*. 2003;4: 397–407.
65. Pyne NJ, Pyne S. Sphingosine 1-phosphate and cancer. *Nat Rev Cancer*. 2010;10: 489–503.
66. Green CD, Maceyka M, Cowart LA, Spiegel S. Sphingolipids in metabolic disease: The good, the bad, and the unknown. *Cell Metab*. 2021;33: 1293–1306.
67. Pitson SM, D'andrea RJ, Vandeleur L, Moretti PA, Xia P, Gamble JR, et al. Human sphingosine kinase: purification, molecular cloning and characterization of the native and recombinant enzymes. *Biochem J*. 2000;350 Pt 2: 429–441.
68. Maceyka M, Sankala H, Hait NC, Le Stunff H, Liu H, Toman R, et al. SphK1 and SphK2, sphingosine kinase isoenzymes with opposing functions in sphingolipid metabolism. *J Biol Chem*. 2005;280: 37118–37129.
69. Hatoum D, Haddadi N, Lin Y, Nassif NT, McGowan EM. Mammalian sphingosine kinase (SphK) isoenzymes and isoform expression: challenges for SphK as an oncotarget. *Oncotarget*. 2017;8: 36898–36929.
70. French KJ, Schrecengost RS, Lee BD, Zhuang Y, Smith SN, Eberly JL, et al. Discovery and evaluation of inhibitors of human sphingosine kinase. *Cancer Res*. 2003;63: 5962–5969.
71. Johnson KR, Johnson KY, Crellin HG, Ogretmen B, Boylan AM, Harley RA, et al. Immunohistochemical distribution of sphingosine kinase 1 in normal and tumor lung tissue. *J Histochem Cytochem*. 2005;53: 1159–1166.
72. Geffken K, Spiegel S. Sphingosine kinase 1 in breast cancer. *Adv Biol Regul*. 2018;67: 59–65.

73. Olivera A, Kohama T, Edsall L, Nava V, Cu villier O, Poulton S, et al. Sphingosine kinase expression increases intracellular sphingosine-1-phosphate and promotes cell growth and survival. *J Cell Biol.* 1999;147: 545–558.
74. Datta A, Loo SY, Huang B, Wong L, Tan SSL, Tan TZ, et al. SPHK1 regulates proliferation and survival responses in triple-negative breast cancer. *Oncotarget.* 2014;5: 5920–5933.
75. Van Brocklyn JR, Jackson CA, Pearl DK, Kotur MS, Snyder PJ, Prior TW. Sphingosine kinase-1 expression correlates with poor survival of patients with glioblastoma multiforme: roles of sphingosine kinase isoforms in growth of glioblastoma cell lines. *J Neuropathol Exp Neurol.* 2005;64: 695–705.
76. Takabe K, Kim RH, Allegood JC, Mitra P, Ramachandran S, Nagahashi M, et al. Estradiol induces export of sphingosine 1-phosphate from breast cancer cells via ABCG1 and ABCG2. *J Biol Chem.* 2010;285: 10477–10486.
77. Nagahashi M, Ramachandran S, Kim EY, Allegood JC, Rashid OM, Yamada A, et al. Sphingosine-1-phosphate produced by sphingosine kinase 1 promotes breast cancer progression by stimulating angiogenesis and lymphangiogenesis. *Cancer Res.* 2012;72: 726–735.
78. Liang J, Nagahashi M, Kim EY, Harikumar KB, Yamada A, Huang W-C, et al. Sphingosine-1-phosphate links persistent STAT3 activation, chronic intestinal inflammation, and development of colitis-associated cancer. *Cancer Cell.* 2013;23: 107–120.
79. Aoki H, Aoki M, Katsuta E, Ramanathan R, Idowu MO, Spiegel S, et al. Host sphingosine kinase 1 worsens pancreatic cancer peritoneal carcinomatosis. *J Surg Res.* 2016;205: 510–517.
80. Yuza K, Nakajima M, Nagahashi M, Tsuchida J, Hirose Y, Miura K, et al. Different Roles of Sphingosine Kinase 1 and 2 in Pancreatic Cancer Progression. *J Surg Res.* 2018;232: 186–194.
81. Imbert C, Montfort A, Fraise M, Marcheteau E, Gilhodes J, Martin E, et al. Resistance of melanoma to immune checkpoint inhibitors is overcome by targeting the sphingosine kinase-1. *Nat Commun.* 2020;11: 437.
82. Song L, Xiong H, Li J, Liao W, Wang L, Wu J, et al. Sphingosine kinase-1 enhances resistance to apoptosis through activation of PI3K/Akt/NF- κ B pathway in human non-small cell lung cancer. *Clin Cancer Res.* 2011;17: 1839–1849.
83. Gachechiladze M, Tich T, Kolek V, Grygrkov I, Klein J, Mgebrishvili G, et al. Sphingosine kinase-1 predicts overall survival outcomes in non-small cell lung cancer patients treated with carboplatin and navelbine. *Oncology Letters.* 2019. doi:10.3892/ol.2019.10447
84. Paugh SW, Paugh BS, Rahmani M, Kapitonov D, Almenara JA, Kordula T, et al. A selective sphingosine kinase 1 inhibitor integrates multiple molecular therapeutic targets in human leukemia. *Blood.* 2008;112: 1382–1391.
85. Ren S, Xin C, Pfeilschifter J, Huwiler A. A novel mode of action of the putative sphingosine kinase inhibitor 2-(p-hydroxyanilino)-4-(p-chlorophenyl) thiazole (SKI II): induction of lysosomal sphingosine kinase 1 degradation. *Cell Physiol Biochem.* 2010;26: 97–104.
86. Gao P, Peterson YK, Smith RA, Smith CD. Characterization of isoenzyme-selective inhibitors of human sphingosine kinases. *PLoS One.* 2012;7: e44543.
87. Houck JD, Dawson TK, Kennedy AJ, Kharel Y, Naimon ND, Field SD, et al. Structural Requirements and Docking Analysis of Amidine-Based Sphingosine Kinase 1 Inhibitors Containing Oxadiazoles. *ACS Med Chem Lett.* 2016;7: 487–492.

88. Yano K. Lipid metabolic pathways as lung cancer therapeutic targets: A computational study. *International Journal of Molecular Medicine*. 2012. pp. 519–529. doi:10.3892/ijmm.2011.876
89. DuPage M, Dooley AL, Jacks T. Conditional mouse lung cancer models using adenoviral or lentiviral delivery of Cre recombinase. *Nat Protoc*. 2009;4: 1064–1072.
90. Ran FA, Hsu PD, Wright J, Agarwala V, Scott DA, Zhang F. Genome engineering using the CRISPR-Cas9 system. *Nat Protoc*. 2013;8: 2281–2308.
91. Suarez-Arnedo A, Torres Figueroa F, Clavijo C, Arbeláez P, Cruz JC, Muñoz-Camargo C. An image J plugin for the high throughput image analysis of in vitro scratch wound healing assays. *PLoS One*. 2020;15: e0232565.
92. Tan SSL, Khin LW, Wong L, Yan B, Ong CW, Datta A, et al. Sphingosine kinase 1 promotes malignant progression in colon cancer and independently predicts survival of patients with colon cancer by competing risk approach in South asian population. *Clin Transl Gastroenterol*. 2014;5: e51.
93. Kawamori T, Osta W, Johnson KR, Pettus BJ, Bielawski J, Tanaka T, et al. Sphingosine kinase 1 is up-regulated in colon carcinogenesis. *FASEB J*. 2006;20: 386–388.
94. Brinkman EK, Chen T, Amendola M, van Steensel B. Easy quantitative assessment of genome editing by sequence trace decomposition. *Nucleic Acids Res*. 2014;42: e168.
95. Kleinman HK, Kim K, Kang H. Matrigel uses in cell biology and for the identification of thymosin β 4, a mediator of tissue regeneration. *Applied Biological Chemistry*. 2018. pp. 703–708. doi:10.1007/s13765-018-0400-6
96. Acharya S, Yao J, Li P, Zhang C, Lowery FJ, Zhang Q, et al. Sphingosine Kinase 1 Signaling Promotes Metastasis of Triple-Negative Breast Cancer. *Cancer Res*. 2019;79: 4211–4226.
97. Meylan E, Dooley AL, Feldser DM, Shen L, Turk E, Ouyang C, et al. Requirement for NF-kappaB signalling in a mouse model of lung adenocarcinoma. *Nature*. 2009;462: 104–107.
98. Kortlever RM, Sodir NM, Wilson CH, Burkhart DL, Pellegrinet L, Brown Swigart L, et al. Myc Cooperates with Ras by Programming Inflammation and Immune Suppression. *Cell*. 2017;171: 1301–1315.e14.
99. Chen N, Fang W, Lin Z, Peng P, Wang J, Zhan J, et al. KRAS mutation-induced upregulation of PD-L1 mediates immune escape in human lung adenocarcinoma. *Cancer Immunol Immunother*. 2017;66: 1175–1187.
100. Breitenecker K, Homolya M, Luca AC, Lang V, Trenk C, Petroczi G, et al. Down-regulation of A20 promotes immune escape of lung adenocarcinomas. *Sci Transl Med*. 2021;13. doi: 10.1126/scitranslmed.abc3911
101. Radisky DC. Epithelial-mesenchymal transition. *Journal of Cell Science*. 2005. pp. 4325–4326. doi:10.1242/jcs.02552
102. Grada A, Otero-Vinas M, Prieto-Castrillo F, Obagi Z, Falanga V. Research Techniques Made Simple: Analysis of Collective Cell Migration Using the Wound Healing Assay. *J Invest Dermatol*. 2017;137: e11–e16.
103. Novikov NM, Zolotaryova SY, Gautreau AM, Denisov EV. Mutational drivers of cancer cell migration and invasion. *Br J Cancer*. 2021;124: 102–114.
104. McGrath JL. Cell spreading: the power to simplify. *Current biology: CB*. 2007. pp. R357–8.

105. Bhat AA, Uppada S, Achkar IW, Hashem S, Yadav SK, Shanmugakonar M, et al. Tight Junction Proteins and Signaling Pathways in Cancer and Inflammation: A Functional Crosstalk. *Front Physiol.* 2018;9: 1942.
106. Liu S, Xu C, Wu W, Fu Z, He S, Qin M, et al. Sphingosine kinase1 promotes the metastasis of colorectal cancer by inducing the epithelial–mesenchymal transition mediated by the FAK/AKT/MMPs axis. *International Journal of Oncology.* 2018. doi:10.3892/ijo.2018.4607
107. Moll HP, Pranz K, Musteanu M, Brcic L, Popper H, Moldvay J, et al. Abstract 809: Afatinib restrains K-RAS driven lung tumorigenesis. *Cancer Research.* 2018. pp. 809–809. doi: 10.1158/1538-7445.am2018-809
108. Haddadi N, Lin Y, Simpson A, Nassif N, McGowan E. “Dicing and Splicing” Sphingosine Kinase and Relevance to Cancer. *International Journal of Molecular Sciences.* 2017. p. 1891. doi:10.3390/ijms18091891
109. Huang Z, Su W, Lu T, Wang Y, Dong Y, Qin Y, et al. First-Line Immune-Checkpoint Inhibitors in Non-Small Cell Lung Cancer: Current Landscape and Future Progress. *Front Pharmacol.* 2020;11: 578091.

Supplementary figures

Figure S1. Fluorescent wound-healing assay. KP cells expressing dTomanto (KPr) and KP Δ SK1 expressing GFP (KP Δ SK1_GFP) were co-cultured for 48 h after initial scratch (0 h time point). Compared to KPr cells, KP Δ SK1_GFP exhibited random movement with lack of cellular sheet formation.

